The Canadian Mineralogist
Vol. 48, pp. 1171-1193 (2010)
DOI: 10.3749/canmin.48.5.1171

MENZERITE-(Y), A NEW SPECIES, $\{(Y,REE)(Ca,Fe^{2+})_2\}[(Mg,Fe^{2+})(Fe^{3+},Al)](Si_3)O_{12}$, FROM A FELSIC GRANULITE, PARRY SOUND, ONTARIO, AND A NEW GARNET END-MEMBER, $\{Y_2Ca\}[Mg_2](Si_3)O_{12}$

EDWARD S. GREW[§], JEFFREY H. MARSH AND MARTIN G. YATES

Department of Earth Sciences, University of Maine, 5790 Bryand Global Sciences Center, Orono, Maine 04469, USA

BILJANA LAZIC AND THOMAS ARMBRUSTER

Mineralogical Crystallography Institute of Geological Sciences, University of Bern, Freiestrasse 3,
CH–3012 Bern, Switzerland

ANDREW LOCOCK

Department of Earth and Atmospheric Sciences, University of Alberta, 1–26 Earth Sciences Building,
Edmonton, Alberta T6G 2E3, Canada

SAMUEL W. BELL

Department of Geology, Amherst College, Amherst, Massachusetts 01002, USA

M. DARBY DYAR

Department of Astronomy, Mount Holyoke College, Kendade Hall, 50 College Street,
South Hadley, Massachusetts 01075, USA

HEINZ-JÜRGEN BERNHARDT

Zentrale Elektronen-Mikrosonde, Institut für Geologie, Mineralogie und Geophysik,
Ruhr-Universität Bochum, D–44801 Bochum, Germany

OLAF MEDENBACH

Institut für Geologie, Mineralogie und Geophysik – Mineralogie, Ruhr-Universität Bochum, D–44780 Bochum, Germany

ABSTRACT

Menzerite-(Y), a new mineral species, forms reddish brown cores, $n = 1.844$ (20), up to 70 μm across, rimmed successively by euhedral almandine containing up to 2.7 wt% Y_2O_3 and by K-feldspar in a felsic granulite on Bonnet Island in the interior Parry Sound domain, Grenville Orogenic Province, Canada. It is named after Georg Menzer (1897–1989), the German crystallographer who solved the crystal structure of garnet. Single-crystal X-ray-diffraction results yielded space group $Ia\overline{3}d$, $a = 11.9947(6)$ Å. An electron-microprobe analysis of the grain richest in Y (16.93 wt% Y_2O_3) gave the following formula, normalized to eight cations and 12 oxygen atoms: $\{Y_{0.83}Gd_{0.01}Dy_{0.05}Ho_{0.02}Er_{0.07}Tm_{0.01}Yb_{0.06}Lu_{0.02}Ca_{1.37}Fe^{2+}_{0.49}Mn_{0.07}\}$ $[Mg_{0.55}Fe^{2+}_{0.42}Fe^{3+}_{0.58}Al_{0.35}V_{0.01}Sc_{0.01}Ti_{0.08}](Si_{2.82}Al_{0.18})O_{12}$, or $\{(Y,REE)(Ca,Fe^{2+})_2\}[(Mg,Fe^{2+})(Fe^{3+},Al)](Si_3)O_{12}$. Synchrotron micro-XANES data gave $Fe^{3+}/\Sigma Fe = 0.56(10)$ *versus* 0.39(2) calculated from stoichiometry. The scattering power refined at the octahedral *Y* site, 17.68 *epfu*, indicates that a relatively light element contributes to its occupancy. Magnesium, as determined by electron-microprobe analyses, would be a proper candidate. In addition, considering the complex occupancy of this site, the average *Y*–O bond length of 2.0244(16) Å is in accord with a partial occupancy by Mg. The dominance of divalent cations with $Mg > Fe^{2+}$ and the absence of Si at the octahedral *Y* site (in square brackets) are the primary criteria for distinguishing menzerite-(Y) from other

---

[§] *E-mail address*: esgrew@maine.edu

silicate garnet species; the menzerite-(Y) end-member is $\{Y_2Ca\}[Mg_2](Si_3)O_{12}$. The contacts of menzerite-(Y) with almandine are generally sharp and, in places, cuspate. It is interpreted to have equilibrated with ferrosilite, augite, quartz, oligoclase, allanite-(Ce), magnetite, ilmenite and fluorapatite, in the absence of almandine, on the prograde path at 7–8.5 kbar and $T \approx$ 700–800°C, and subsequently dissolved incongruently in an anatectic melt to form almandine, most likely, at $P \approx$ 8.5–9.5 kbar and $T \approx$ 800–850°C.

Keywords: garnet, menzerite, yttrium, rare-earth elements, new mineral species, crystal structure, Grenville Province, granulite facies, Parry Sound, Ontario.

SOMMAIRE

La menzerite-(Y), nouvelle espèce minérale, se présente en noyaux bruns rougeâtres, n = 1.844 (20), jusqu'à 70 μm de diamètre, entourés successivement par l'almandin idiomorphe contenant jusqu'à 2.7% Y_2O_3 (poids) et par le feldspath potassique dans une granulite felsique sur l'île Bonnet, faisant partie du domaine interne de Parry Sound, province orogénique du Grenville, au Canada. Le nom rappelle Georg Menzer (1897–1989), cristallographe allemand qui a été le premier à résoudre la structure cristalline du grenat. Nos résultats obtenus par diffraction X sur monocristal indiquent le groupe spatial $Ia\overline{3}d$, a = 11.9947(6) Å. Une analyse du grain le plus riche en Y (16.93% Y_2O_3) avec une microsonde électronique mène à la formule suivante, normalisée selon huit cations et 12 atomes d'oxygène: $\{Y_{0.83}Gd_{0.01}Dy_{0.05}Ho_{0.02}Er_{0.07}Tm_{0.01}Yb_{0.06}Lu_{0.02}Ca_{1.37}Fe^{2+}_{0.49}Mn_{0.07}\}[Mg_{0.55}Fe^{2+}_{0.42}Fe^{3+}_{0.58}Al_{0.35}V_{0.01}Sc_{0.01}Ti_{0.08}](Si_{2.82}Al_{0.18})O_{12}$ ou, de façon idéale, $\{(Y,REE)(Ca,Fe^{2+})_2\}[(Mg,Fe^{2+})(Fe^{3+},Al)](Si_3)O_{12}$. Les données micro-XANES obtenues avec un synchrotron indiquent $Fe^{3+}/\Sigma Fe$ = 0.56(10) *versus* 0.39(2), valeur calculée par stoechiométrie. Le pouvoir de dispersion affiné au site octaédrique Y, 17.68 *epfu*, indique qu'un élément relativement léger loge à ce site. Le magnésium, tel que déterminé par analyse avec une microsonde électronique, serait un candidat approprié. De plus, compte tenu de la complexité des occupants de ce site, la longueur de la liaison Y–O moyenne, 2.0244(16) Å, concorde avec un taux d'occupation partiel par le Mg. La prédominance des cations bivalents, avec $Mg > Fe^{2+}$, et l'absence du Si au site octaédrique Y (entre crochets carrés), seraient les principaux critères pour distinguer la menzerite-(Y) des autres espèces de grenat silicaté; le pôle menzerite-(Y) possède une composition $\{Y_2Ca\}[Mg_2](Si_3)O_{12}$. Les contacts entre la menzerite-(Y) et l'almandin sont francs, en général, et cuspidés par endroits. Ce grenat aurait été équilibré avec ferrosilite, augite, quartz, oligoclase, allanite-(Ce), magnétite, ilménite et fluorapatite, en l'absence de l'almandin, au cours du tracé prograde à 7–8.5 kbar et à environ 700–800°C, et par la suite aurait été dissout de manière incongruente dans un bain fondu anatectique pour former l'almandin, très probablement à une pression voisine de 8.5–9.5 kbar et à environ 800–850°C.

(Traduit par la Rédaction)

Mots-clés: grenat, menzerite, yttrium, terres rares, nouvelle espèce minérale, structure cristalline, Province de Grenville, faciès granulite, Parry Sound, Ontario.

INTRODUCTION

Yttrium and the heavy rare-earth elements (HREE) were first revealed to be important constituents of garnet by Jaffe (1951) and Yoder & Keith (1951). Currently, Y and the HREE receive considerable attention not only as sensitive indicators of garnet growth and resorption history (*e.g.*, Lanzirotti 1995, Pyle & Spear 1999), but also because such histories may be related to the growth of minerals such as zircon, thus providing a means of dating the stages of metamorphic evolution (*e.g.*, Rubatto & Hermann 2007, Harley & Kelley 2007). The yttrium contents of common metamorphic and plutonic garnets typically range from several tens of ppm to several thousand ppm (*e.g.*, Lanzirotti 1995, Pyle & Spear 1999), and commonly exceed the yttrium contents of associated rock-forming minerals by an order of magnitude or more (Bea 1996). In a few pegmatitic occurrences of garnet, Y contents reach 24800–26500 ppm (3.15–3.36 wt% Y_2O_3, Enami *et al.* 1995, Kasowski & Hogarth 1968), corresponding to 0.14–0.15 Y per formula unit (on the basis of eight cations and 12 oxygen atoms).

Here, we describe a garnet-group mineral containing up to 17 wt% Y_2O_3 as the new species menzerite-(Y) and report its crystal structure, which provides the critical information on site occupancies needed to distinguish menzerite-(Y) from other garnet species. The mineral and name were approved by the Commission on New Minerals, Nomenclature and Classification of the International Mineralogical Association (IMA 2009–050). It is named after the crystallographer Georg Menzer (1897–1989), Professor at the Ludwig-Maximilians-Universität München, who was the first to solve the structure of garnet, and in fact the first to solve the structure of a silicate mineral (Menzer 1925, 1926, 1928, Laves 1962). The Levinson modifier, -(Y), attests to the dominance of Y over the rare-earth elements present.

The holotype material (sample no. GB50, part A and thin section GB50A1, collected in 2008) was deposited in the Canadian Museum of Nature, P.O. Box 3443, Station D, Ottawa, Ontario, Canada K1P 6P4, as catalogue number CMNMC 86088; a second sample (GB94, part I, billet 4, collected in 2009) from the type locality is deposited in the National Museum of Natural History, Smithsonian Institution, Washington, D.C., as catalogue number NMNH 174896. Sections from samples GB50 and GB94 were used in the present study.

OCCURRENCE

Menzerite-(Y) occurs sparingly as an accessory mineral included in euhedral almandine (Fig. 1) in felsic granulite on the north shore of Bonnet Island in Georgian Bay, offshore from the town of Parry Sound, Ontario, Canada (UTM coordinates 0567531W 5003719N; NAD 83 datum, zone 17). Bonnet Island is an exposure of well-layered granulite-facies supracrustal rocks in the interior Parry Sound Domain, Grenville Province, and is part of an allochthonous terrane that is near the highest structural level of a stack of thrust nappes assembled at around 1120–1090 Ma (Davidson *et al*. 1982, Culshaw *et al*. 1997).

ANALYTICAL METHODS

Optical properties

The optical properties of menzerite-(Y) were measured on grain #1 in section GB50A1 at the Ruhr-Universität Bochum. Reflectance measurements were made in air and oil (DIN 58 884, index of refraction of oil: 1.518 at 23°C) with light of wavelength 580 nm, and the index of refraction of menzerite-(Y) was calculated using Beer's Law. The standard used was SiC.

X-ray diffraction

A single-crystal X-ray-diffraction study was carried out at the University of Bern using an APEX II SMART diffractometer. We used commercial software for intensity retrieval from 3D CCD-frame data as supplied by the producer of the instrument. This software does not allow peak deconvolution or other sophisticated profile treatment procedures.

A composite grain (#2 in section GB50A1, Fig. 1) was extracted from the thin section using a drill mounted on a microscope (Medenbach 1986). The sample was found to consist of menzerite-(Y) flanked on two sides by almandine, which by visual inspection constituted about 50% of the composite grain (Fig. 2, inset). We tried the micro-milling technique as a way to remove the enclosing almandine, because the impact of this mechanical treatment on the crystal structure would be less severe than other techniques of separation like laser ablation or electron bombardment. Unfortunately, applying the micro-milling technique turned out to be more difficult than anticipated because the three-dimensional intergrowth was more complex than initially believed from two-dimensional pictures.

Table 1 summarizes the conditions under which the single-crystal data were collected. A plot of reciprocal space shows that the two superimposed cubic lattices are perfectly aligned; the reflections for almandine and menzerite-(Y) are clearly distinguished as a result of the difference in their unit-cell dimensions (Fig. 2). For each pair of corresponding reflections, those at slightly higher *d*-values were manually assigned to menzerite-(Y), and those with smaller *d*-values, to almandine. Each diffraction spot is shown simply as a circle with its center at the center of gravity (intensity) of an observed reflection; the circles are not intended to show the true shape of a diffraction spot, but only its ideal position in a projection of reciprocal space. Thus, Figure 2 does not indicate whether the shoulders of corresponding reflections overlap or whether individual reflections from the two fragments are completely resolved. This figure shows that below a Bragg angle θ (Mo$K\alpha$ radiation) of ~17° (corresponding to the 10 0 0 reflection), even and odd reflection indices fulfilling *I*-centering are observed. At higher θ values, observed reflections with odd indices and $h + k + l = 2n$ become scarce. In the garnet structure, all cations at the *X*, *Y*, and *Z* sites are on special positions associated with the reflection conditions: *hkl*: $h, k = 2n, h + k + l = 4n$. Only oxygen occupies a general position, permitting intensities with odd indices. These extinction rules require us to rely on the low-θ angle reflections, even though they are much more affected by mutual overlap than those at high θ angles. The orientation matrices were determined from the reflections assigned either to menzerite-(Y) or almandine based on preliminary unit-cell dimensions a equal to 12.00 Å and 11.66 Å, respectively. These parameters were used for integration of the reflection intensities. In order to reduce the effect of mutual overlap of the reflections, we used a fixed narrow box-size with x = y = 0.5° and z = 1° for integration. The box size was chosen by trial and error. A narrow box-width has the disadvantage that strong reflections suffer from substantial truncation of the flanks. If the box-size refinement option in the intensity-integration software were enabled or if the selected dimensions of the box were too large, the integrated intensity would include contributions from both reflections, and the final cell-dimension refinement would converge to be an average of menzerite-(Y) and almandine. In summary, because of partial overlap of reflections from menzerite-(Y) and almandine at low θ angles and truncation of the strongest reflections, the diffraction data are of mediocre quality, and the parameters R_{int} and R_{s} are very different (Table 1). This precludes any quantitative analysis of the displacement parameters.

For the refinement of menzerite-(Y), we used the scattering factors of Y and Ca for the *X* site, those of Al and Fe for the *Y* site, and the *Z* site was constrained to be fully occupied by Si in order to reduce correlations between the scale factor and site occupancies. For the refinement of almandine, we used the scattering factors of Fe and Ca for the *X* site, those of Al

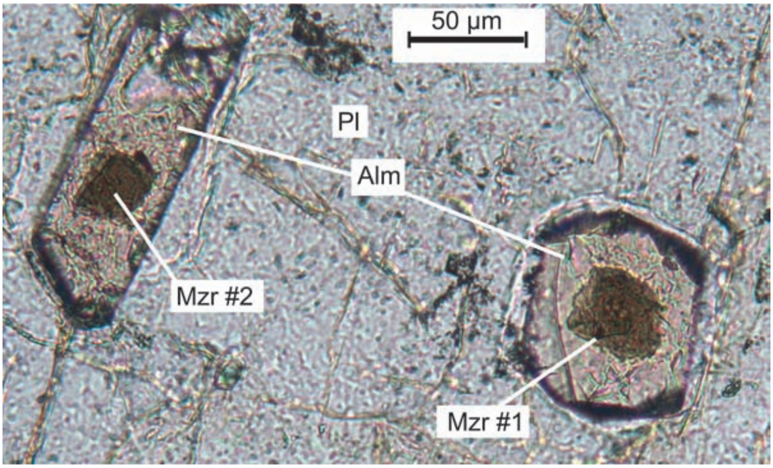

FIG. 1. Photomicrograph of grains of menzerite-(Y) used for single-crystal (#2) and optical study (#1). Plane-polarized light.

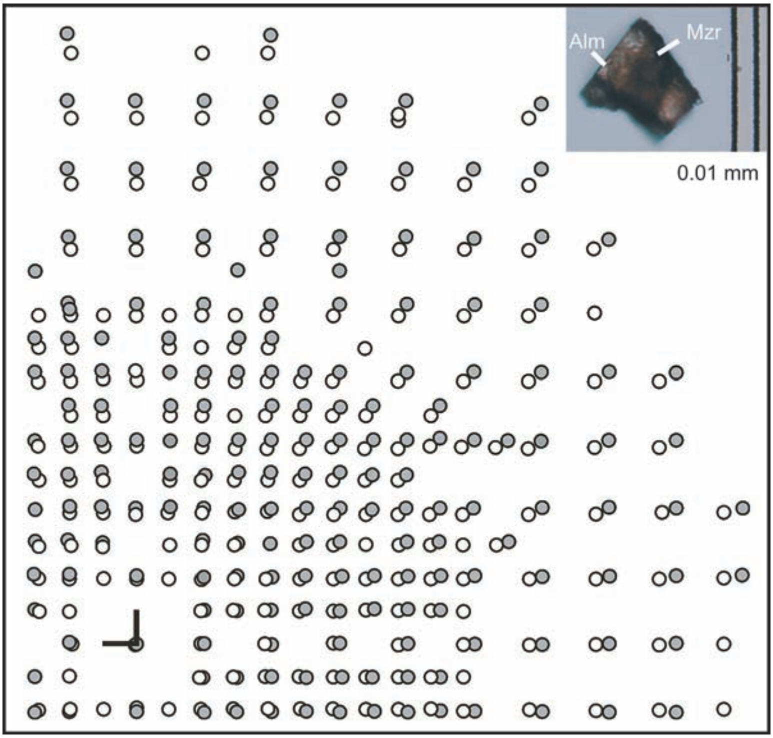

FIG. 2. Projection along a^* of reciprocal space showing separation of menzerite-(Y) reflections [unfilled circles, a = 11.9947(6) Å] from almandine reflections [gray filled circles, a = 11.6598(8) Å]. Inset shows grain #2, section GB50A1 from which the pattern was obtained; spacing between the bars is 0.01 mm.

and Fe for the *Y* site, and the *Z* site was constrained to be fully occupied by Si. Assignment of these "dummy atoms" allowed determination of the average site-scattering values, which can be compared to the results of the electron-microprobe analysis (Table 2). The final refinements were performed with anisotropic displacement parameters for all sites. A table showing these parameters is available from the Depository of Unpublished Data on the MAC website [document Menzerite-(Y) CM48_1171]. Comparison of the scale factors confirmed that the rim of almandine and the core of menzerite-(Y) contributed in nearly equal parts to the composite crystal in terms of weight percent.

Because of the possible overlap of the menzerite and almandine data, we compare the site-scattering values from the single-crystal refinement (SREF) and results of the electron-microprobe analyses (EMPA) in order to determine whether the site occupancies obtained for menzerite-(Y) were affected by almandine and *vice versa*. Comparison of the data in Table 2 shows that the site-scattering values for the *X* site from the SREF and EMPA are in good agreement for both menzerite-(Y) and almandine, as are the site-scattering values for the *Y* site in almandine, *i.e.*, the differences are 2–4% of the measured values, similar to the esd values of the SREF site-scattering values. The SREF and EMPA site-scattering differs by 9.5% for the *Y* site in menzerite-(Y), a discrepancy attributed to chemical zoning in menzerite-(Y) (see below) and to the fact that the SREF is based on the entire volume of the extracted crystal, whereas EMPA is based on a small volume at the center of the crystal. In summary, we are confident that overlap of reflections is sufficiently low to avoid ending up with an average occupancy between menzerite-(Y) and almandine. Further justification for our confidence is the substantial difference of 5.2 electrons per formula unit in site scattering between menzerite-(Y) and almandine at the *X* site (Table 2).

To validate the reliability in our oxygen coordinates, we have performed a simple test by assuming that almandine surrounding menzerite has a simplified composition of 26.0% grossular, 62.3% almandine, and 11.7% pyrope. These approximate numbers are obtained if the low Y content is considered as grossular-like, and the Mn^{2+} content, as almandine-like. Oxygen coordinates for this solid-solution member are calculated as linear combinations of the corresponding oxygen coordinates of the end members (RT data) for

TABLE 1. DETAILS OF THE SINGLE-CRYSTAL X-RAY STRUCTURE REFINEMENTS OF MENZERITE-(Y) AND ALMANDINE*

Grain shape	prism
Grain size (mm)	0.040 × 0.030 × 0.040
Diffractometer	APEX II SMART
X-ray radiation	Mo $K\alpha$ (λ = 0.71073 Å)
X-ray power	50 kV, 30 mA
Monochromator	graphite
Temperature	293 K
Detector-to-sample distance	4 cm
Measurement method	omega scans
Rotation width	0.5°
Total number of frames	1289
Frame size	512 × 512 pixels
Time per frame	60 seconds

	Menzerite-(Y)	**Almandine**
Unit-cell dimension *a* (Å)	11.9947(6)	11.6598(8)
Volume ($Å^3$)	1725.71(15)	1585.2(2)
Space group	$Ia\bar{3}d$ (No. 230)	$Ia\bar{3}d$ (No. 230)
Z	8	8
θ range for data collection	4.16 to 42.50°	4.28 to 42.43°
Index ranges	$-20 \le h \le 22$ $-19 \le k \le 22$ $-22 \le l \le 20$	$-18 \le h \le 21$ $-20 \le k \le 22$ $-20 \le l \le 21$
No. of measured reflections	16788	15335
No. of unique reflections	525	483
No. of observed reflections [$I > 2\sigma(I)$]	267	257
No. of parameters	19	19
R_{int}	0.1140	0.0862
R_s	0.0372	0.0264
$R1$, $I > 2\sigma(I)$	0.0301	0.0523
$R1$, all data	0.0916	0.0971
$wR2$ / $wR2$ all data (on F^2)	0.0441 /0.0579	0.1298/ 0.1614
GooF	1.051	1.015
$\Delta\rho_{min}$ ($-e$ Å^{-3})	−0.838 close to ^{Z}Si	−1.952 close to ^{Z}Si
$\Delta\rho_{max}$ (e Å^{-3})	0.742 close to ^{X}Y	1.141 close to ^{X}Fe

* For a grain containing both minerals.

grossular (Geiger & Armbruster 1997), almandine and pyrope (Armbruster *et al.* 1992). This approach yielded a predicted O coordinate of x = 0.0350, y = 0.0482, z = 0.6525, which agrees within 3.5 esd or less with the refined coordinates (Table 3). Considering the simplicity of the model, the agreement is excellent.

X-ray absorption spectroscopy

Given the ambiguities in determining site occupancies and the valences of V, Cr, Mn, and Fe, and in measuring the H content in a complex garnet solid-solution, it would have been desirable to supplement the crystal-structure refinements and electron-microprobe analyses with infrared, visible-light, and Mössbauer spectroscopic measurements (Geiger 2004). However, the menzerite-(Y) grains are sparse (no more than 10–12 grains per thin section), very fine (mostly <50 μm) and, with rare exceptions, enclosed in almandine, leaving X-ray absorption spectroscopy near the absorption edge on a microscopic scale (micro-XANES, Dyar *et al.* 2002, Mottana 2004) as the only practical method for the material at hand. Optical spectroscopy from the near-ultraviolet through visible into the infrared of the largest menzerite-(Y) grains is in theory also possible because spot sizes as small as "on the order of 20 μm" have been achieved (Wildner *et al.* 2004), but this would require very challenging sample preparation and specialized instrumentation that is beyond the scope of the present study.

Thus, XANES spectra were acquired at beamline X26A at the National Synchrotron Light Source at Brookhaven National Laboratory using an 8 × 10 μm beam size. Incident X-rays were tuned using a Si(311) monochromator. The XANES spectra were collected in fluorescence mode using a nine-element high-purity Ge solid-state detector array. Data were acquired from the centers and edges of two grains. Spectra were edge-step-normalized and corrected for self-absorption using the FLUO algorithm. Energies were calibrated using a magnetite standard, where the position of the pre-edge peak is known precisely. A function was fit in the region of the pre-edge to approximate the upwardly sloping main edge, and then subtracted. Lorentzian functions

TABLE 2. COMPARISON OF SITE OCCUPANCIES AND SCATTERING, MEASURED OR CALCULATED FROM ELECTRON-MICROPROBE DATA (EMPA) AND FROM SINGLE-CRYSTAL STRUCTURE REFINEMENT (SREF), OF MENZERITE-(Y) GRAIN #2 AND ENCLOSING ALMANDINE GRAIN 3b2, SECTION GB50A1

	Menzerite-(Y)					Almandine			
	Occupancy (apfu)		Site scattering			Occupancy (apfu)		Site scattering	
Method	EMPA	SREF	EMPA	SREF		EMPA	SREF	EMPA	SREF
Ca*	1.495	1.47(2)	9.966	9.8(2)	Ca*	0.726	0.80(6)	4.84	5.4(4)
Y	0.655		8.515						
Fe^{2+}	0.600		5.200		Y	0.048		0.62	
Mn	0.034		0.250		Fe^{2+}	1.756		15.22	
Gd	0.012		0.256		Mn	0.117		0.98	
Dy	0.042		0.924		Gd	0.003		0.06	
Ho	0.014		0.322		Er	0.007		0.16	
Er	0.072		1.632		Yb	0.008		0.19	
Yb	0.063		1.400		Mg	0.332		1.33	
Sum*	1.492	1.53(2)	18.499	19.9(5)	Sum*	2.271	2.20(6)	18.56	19.0(5)
Total *X*	2.987	3	28.465	29.7	Total *X*	2.997	3	23.400	24.4
Al	0.326		2.106		Al	1.855	1.808(19)	12.058	11.75(12)
Mg	0.558		3.384						
Sum*	0.884	1.189(14)	5.490	7.13(9)	Sum*	1.855	1.808(19)	12.058	11.75(12)
Fe^{3+}	0.672		8.736		Fe^{3+}	0.086		1.1185	
Fe^{2+}	0.291		3.744		Fe^{2+}	0.050		0.6505	
Ti	0.103		1.056		V	0.005		0.0552	
V	0.027		0.267		Ti	0.003		0.0360	
Sc	0.023		0.252		Cr	0.001		0.0115	
Sum*	1.116	0.811(14)	14.055	10.55(19)	Sum	0.145	1.192(19)	1.8717	2.50(25)
Total *Y*	2	2	19.545	17.68	Total *Y*	2	2	13.9297	14.25
Si *	2.874		13.44	14	Si *	2.979	3	13.888	14
Al	0.126		0.52		Al	0.021		0.104	
Total *Z*	3	3	13.96	14	Total *Z*	3	3	13.992	14

Note: apfu: atoms per formula unit. * These SREF values correspond to the "dummy atoms" mentioned in the text.

were fit to the individual peaks in the pre-edge using the PAN peak-fitting software written by R.M. Dimeo at the NIST Center for Neutron Research. The positions (energies) and calculated peak-areas were used to create a weighted peak-center for each spectrum. Several other garnet standards with known Fe^{3+}/ΣFe were also measured, and a calibration curve relating the weighted peak-center energies to Fe^{3+}/ΣFe was created. This expression was then used to determine the Fe^{3+}/ΣFe in menzerite-(Y) and the surrounding almandine. The interpretation of spectra obtained on single crystals of garnet is not affected by orientation, because garnet is isometric, and there is no contribution to the errors from polarization effects (Dyar *et al.* 2002). Further information on this calibration will be reported in Dyar *et al.* (in prep.). The data reported in the present paper are preliminary pending further refinement of that calibration.

Electron-microprobe analysis

Menzerite-(Y) and almandine in samples GB50 and GB94 were analyzed with a Cameca SX–100 electron microprobe using wavelength-dispersive spectroscopy (WDS) at the University of Maine. A special protocol was developed for menzerite-(Y), but the final method was developed only after grain #2 in section GB50A1 had been extracted for structure refinement. Column conditions in the final method for elements Mg to Y were 15 kV, 10 nA, and 5 µm beam diameter, and for the rare-earth elements (REE), 25 kV, 20 nA, *ca.* 5 µm (focused) beam diameter. The data were processed using the X-Phi correction of Merlet (1994). For menzerite-(Y), we used the following standards (and lines): pyrope (Mg$K\alpha$), synthetic $\{Y_2\}[Al_2](Al_3)O_{12}$ (Al$K\alpha$), zircon (Si$K\alpha$), diopside (Ca$K\alpha$), Sc metal (Sc$K\alpha$), rutile (Ti$K\alpha$), V metal (V$K\alpha$), Cr_2O_3 (Cr$K\alpha$), rhodonite (Mn$K\alpha$), almandine (Fe$K\alpha$); synthetic $\{Y_2\}[Al_2](Al_3)O_{12}$ (Y$L\alpha$), and synthetic $REEP_5O_{14}$ ($L\alpha$ for La, Ce, Nd, Eu, Gd, Tb, Er, Tm, and Yb; $L\beta$ for Pr, Sm, Dy, Ho and Lu). No other element with $Z \geq 5$ was detected in WDS scans. Grain #2 of menzerite-(Y) in section GB50A1, which was used for refinement of the crystal structure, was also analyzed under two different sets of conditions; for elements Mg to Y plus Lu, conditions were 15 kV, 10 nA; for the rare-earth elements except Lu, they were 25 kV, 20 nA, both with a 5 µm beam diameter and the following standards (and lines): pyrope (Mg$K\alpha$), almandine (Al$K\alpha$, Si$K\alpha$, Fe$K\alpha$), diopside (Ca$K\alpha$), Sc metal (Sc$K\alpha$), rutile (Ti$K\alpha$), V metal (V$K\alpha$), rhodonite (Mn$K\alpha$), synthetic $\{Y_2\}[Al_2](Al_3)O_{12}$ (Y$L\alpha$), and synthetic $REEP_5O_{14}$ ($L\alpha$ for La, Ce, Nd, Gd, Tb, Er, Tm and Yb; $L\beta$ for Pr, Sm, Eu, Dy, and Ho; $M\alpha$ for Lu). Analytical totals range from 100.57 to 103.50 wt% with the refined protocol, whereas the total for grain #2 was 97.40 wt%.

TABLE 3. COORDINATES AND EQUIVALENT ISOTROPIC DISPLACEMENT PARAMETERS (Å^2) OF ATOMS IN MENZERITE-(Y) AND ALMANDINE

Atom	*x*/*a*	*y*/*b*	*z*/*c*	U_{eq}	occupancy
			Menzerite-(Y)		
^{X}Ca	0.125	0.0	0.25	0.01200(14)	0.491(8)
^{X}Y	0.125	0.0	0.25	0.01200(14)	0.509(8)
^{Y}Fe	0.0	0.0	0.0	0.0069(2)	0.406(7)
^{Y}Mg	0.0	0.0	0.0	0.0069(2)	0.594(7)
^{Z}Si	0.375	0.0	0.25	0.0091(3)	1.000
O	0.03750(14)	0.05030(14)	0.65668(14)	0.0152(4)	1.000
			Almandine		
^{X}Ca	0.125	0.0	0.25	0.0150(2)	0.268(19)
^{X}Fe	0.125	0.0	0.25	0.0150(2)	0.732(19)
^{Y}Al	0.0	0.0	0.0	0.0113(4)	0.904(10)
^{Y}Fe	0.0	0.0	0.0	0.0113(4)	0.096(10)
^{Z}Si	0.375	0.0	0.25	0.0095(3)	1.000
O	0.03516(15)	0.04794(14)	0.65294(14)	0.0138(4)	1.000
O*	0.0350	0.0482	0.6525		

U_{eq} is one third of the trace of the orthogonalized U_{ij} tensor. * Predicted (see text).

Almandine in section GB50A1 was analyzed for all elements at a single set of conditions, 25 kV, 10 nA, and *ca.* 5 µm (focused) beam diameter. We used as standards (and lines) diopside (Mg$K\alpha$, Ca$K\alpha$), albite (Al$K\alpha$), wollastonite (Si$K\alpha$), rutile (Ti$K\alpha$), V metal (V$K\alpha$), Cr_2O_3 (Cr$K\alpha$), rhodonite (Mn$K\alpha$), almandine (Fe$K\alpha$); synthetic $\{Y_2\}[Al_2](Al_3)O_{12}$ (Y$L\alpha$), and synthetic $REEP_5O_{14}$ ($L\alpha$ for Er and Yb; $L\beta$ for Gd and Dy).

Almandine in sections GB50C and GB94I4 was analyzed for all elements at a single set of conditions, 15 kV, 10 nA, and 5 µm beam diameter. We used standards (and lines) jadeite (Na$K\alpha$), diopside (Mg$K\alpha$, Ca$K\alpha$), almandine (Al$K\alpha$, Si$K\alpha$, Fe$K\alpha$), sanidine (K$K\alpha$), rutile (Ti$K\alpha$), rhodonite (Mn$K\alpha$), and synthetic $\{Y_2\}[Al_2](Al_3)O_{12}$ (Y$L\alpha$).

Menzerite-(Y) in grain 5, section GB50A2 was mapped for Mg, Al, Ca, Ti, Y, Er and Yb with a focused beam at 15 kV and 200 nA using the following crystals: TAP (Mg$K\alpha$, Al$K\alpha$), PET (Ca$K\alpha$, Ti$K\alpha$, Y$L\alpha$), LIF (Yb $L\alpha$, Er $L\alpha$). Titanium, Er and Yb were mapped with two spectrometers simultaneously, and the resulting images were added to one another. Profiles of Mg, Ti, Mn, Y, and Yb concentrations in traverses across eleven grains of menzerite-(Y) and the enclosing almandine in sections GB50A1 and GB50A2 were obtained with a focused beam at 15 kV and 100 nA using the following crystals: TAP (Mg$K\alpha$), PET (Ti$K\alpha$, Y$L\alpha$), LIF (Mn$K\alpha$, Yb$L\alpha$).

MICROSTRUCTURES OF MENZERITE-(Y) AND ALMANDINE

Menzerite-(Y) occurs as an accessory phase in a foliated felsic granulite that has an indistinct compositional layering on a millimeter scale. The most abundant minerals associated with menzerite-(Y) are oligoclase ($An_{25–28}$), quartz, and ferrosilite ($Fs_{56–61}En_{38–43}Wo_{1–3}$ plus ~1% $MnSiO_3$). K-feldspar, augite ($Fs_{27–29}En_{29–30}Wo_{41–43}$), calcic amphibole, biotite, almandine, ilmenite and magnetite are subordinate (Grew *et al.* 2010). Accessory phases include fluorapatite, allanite-(Ce), and zircon, which are widespread, whereas monazite-(Ce), xenotime-(Y), pyrite, chalcopyrite, sphalerite, hercynite, and Mg–Fe carbonate occur very sparsely.

Although mostly isolated from other phases by almandine, menzerite-(Y) is locally in contact with K-feldspar (Figs. 3, 4a) and with several of the other minerals enclosed in almandine: allanite-(Ce) (Fig. 3), ilmenite and fluorapatite (Fig. 5a). No contacts with oligoclase, quartz, ferrosilite or any other mineral were found. Grains of menzerite-(Y) range from equant to elongate, up to 70 μm in the longest dimension. Its contacts are sharp and commonly cuspate or show embayments (Figs. 4a, 4c, 5a). In a few cases, several grains of menzerite-(Y) are enclosed in a single grain of almandine, *e.g.*, the atoll in Figure 5a.

Almandine surrounding menzerite-(Y) is euhedral, in places with smooth faces and sharp corners (Figs. 3, 4a, 4e, 4f), and surrounded by a moat of K-feldspar, locally with quartz (Fig. 5a). In some cases, almandine overgrowing inclusion-poor almandine around menzerite-(Y) contains quartz vermicules (Figs. 4b, 4d). This almandine–quartz symplectite, which can also include augite vermicules, is more common around ferrosilite, magnetite and ilmenite. Almandine also forms a symplectite with biotite in decussate aggregates and quartz in sample GB94I (Grew *et al.* 2010).

Physical Properties, Index of Refraction and Compatibility Index of Menzerite-(Y)

Most of the physical properties of menzerite-(Y) cannot be determined because of the small grain-size and scarcity. Cleavage was not evident. Tenacity is brittle, as shown by a broken grain (Fig. 2 inset). Density, calculated with the empirical formula, is 4.31 g/cm^3 (grain #5 for composition; grain #2 for cell parameters, section GB50A1). Menzerite-(Y) is transparent and isotropic. Reflectance is 8.83% (air), 0.97% (oil), which gives n = 1.844 (20) at 580 nm for grain #1, section GB50A1. The color is deep reddish brown in thin sections of standard thickness (~ 0.03 mm, Fig. 1).

The Gladstone–Dale relation (Mandarino 1981) gives a compatibility index $1 - (K_P/K_C) = 0.003$, excellent; it was calculated using the cell volume, index of refraction and chemical composition from grains #2, #1 and #5 (section GB50A1), respectively.

X-Ray Diffraction Study and Crystal Structure of Menzerite-(Y)

By and large, the site assignments given in Tables 2 and 3 for menzerite-(Y) are consistent with site occupancies in common rock-forming garnets: Ca, Mn, Y and REE at the *X* site, Ti and all trivalent cations at the *Y* site (except minor amounts of Al needed to fill the *Z* site), and Si at the *Z* site. Where menzerite-(Y) differs from more common garnets is in the assignment of the divalent cations Mg and Fe^{2+}. The refinement is consistent with Mg being assigned to *Y* instead of *X*, and with Fe^{2+} being apportioned between the *X* and *Y* sites to bring their occupancies up to three and two cations per formula unit, respectively. Thus, the discussion will focus on justifying the latter two unconventional site-assignments.

The good agreement between EPMA and SREF in site scattering and the high number of electrons (*ca.* 29) at the *X* site argue in favor of assigning Fe^{2+} rather than Mg to *X* to bring its total occupancy to three. If more Fe^{2+} and less Mg were assigned to *Y*, the discrepancy is worsened between the EMPA and SREF site scattering for the *Y* site. Moreover, our assignments are consistent with the radii of Mg and Fe^{2+}: the smaller Mg ion should be partitioned into the smaller of the two sites, *i.e.*, at *Y*. Because there are so few garnet species with substantial divalent-cation occupancy at *Y*, data on the distribution of Mg and Fe^{2+} between *X* and *Y* are sparse and contradictory. On the basis of Mössbauer spectroscopy, Kühberger *et al.* (1989) reported a modest fractionation of Fe^{2+} at the *Y* site relative to the *X* site in schorlomite, but the *X* site is largely occupied by Ca (2.89–2.90 Ca per formula unit). In contrast, Geiger *et al.* (1991a, 1991b) cited Mössbauer data as evidence that Fe^{2+} is strongly fractionated at the *X* site relative to the *Y* site in synthetic Ca-free majorite, an interpretation supportive of our model for menzerite-(Y).

In order to further verify the distribution of cations between *X* and *Y*, we have performed *X*–O and *Y*–O distance predictions based on the composition obtained by EMPA (Table 2). The *X* site is occupied by 50% Ca, 21% Fe^{2+} (including minor Mn^{2+}), and 29% Y (with minor REE). Reference distances were taken from synthetic garnet end-members (Ca–O: andradite, Fe–O: almandine, Y–O: YAG). The calculated *X*–O distances

FIG. 3. Maps of six elements in menzerite-(Y), grain #5, section GB50A2. Back-scattered electron image shows area mapped (white square). The following lines were measured: Al*K*α, Ca*K*α, Ti*K*α, Y*L*α, Er*L*α, and Yb*L*α. Color scales to the right of the images show how the image was adjusted to maximize contrast in the IMAGEJ program. Abbreviations: Alm: almandine, Aln: allanite-(Ce), Kfs: K-feldspar, M: menzerite-(Y), Pl: oligoclase.

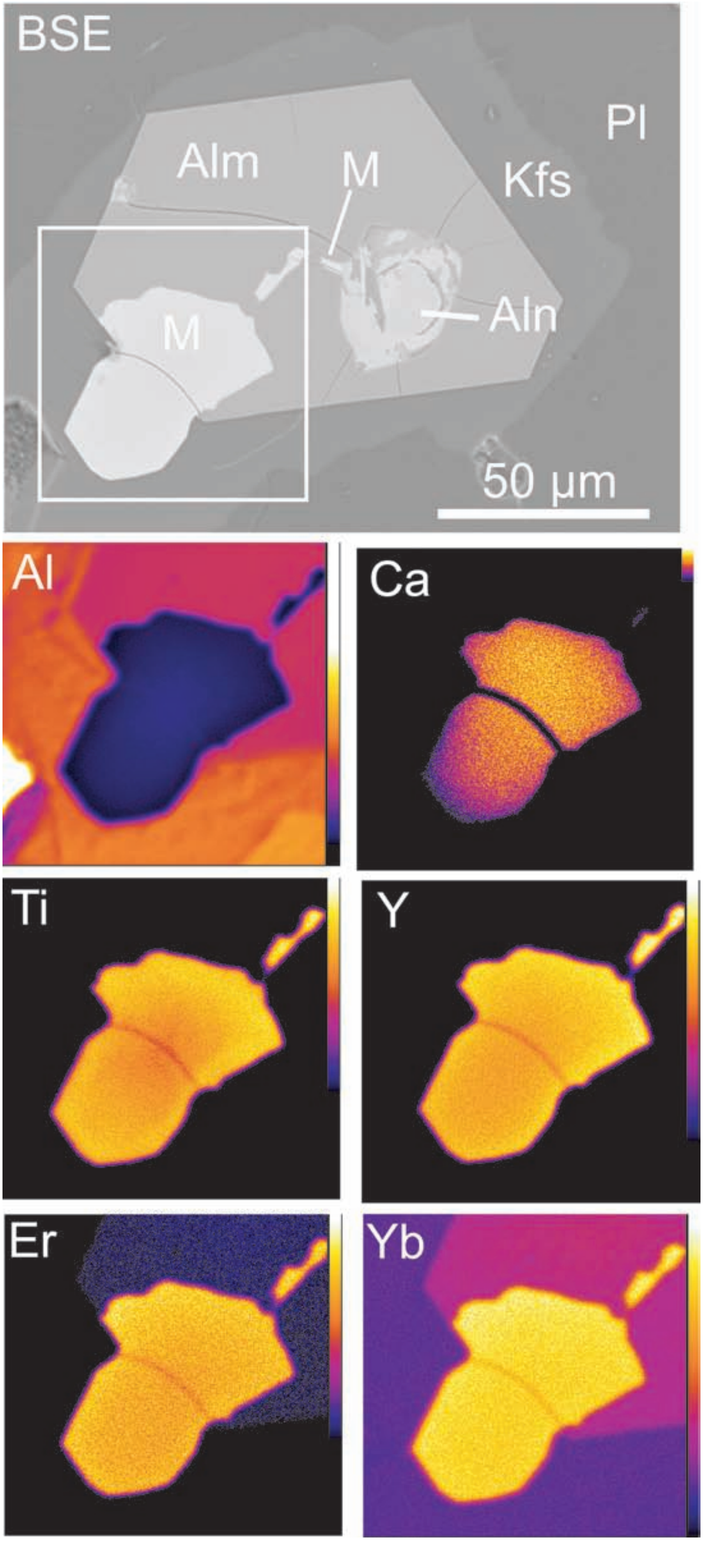
BSE
Pl
Alm
M
Kfs
M
Aln
50 µm
Al
Ca
Ti
Y
Er
Yb

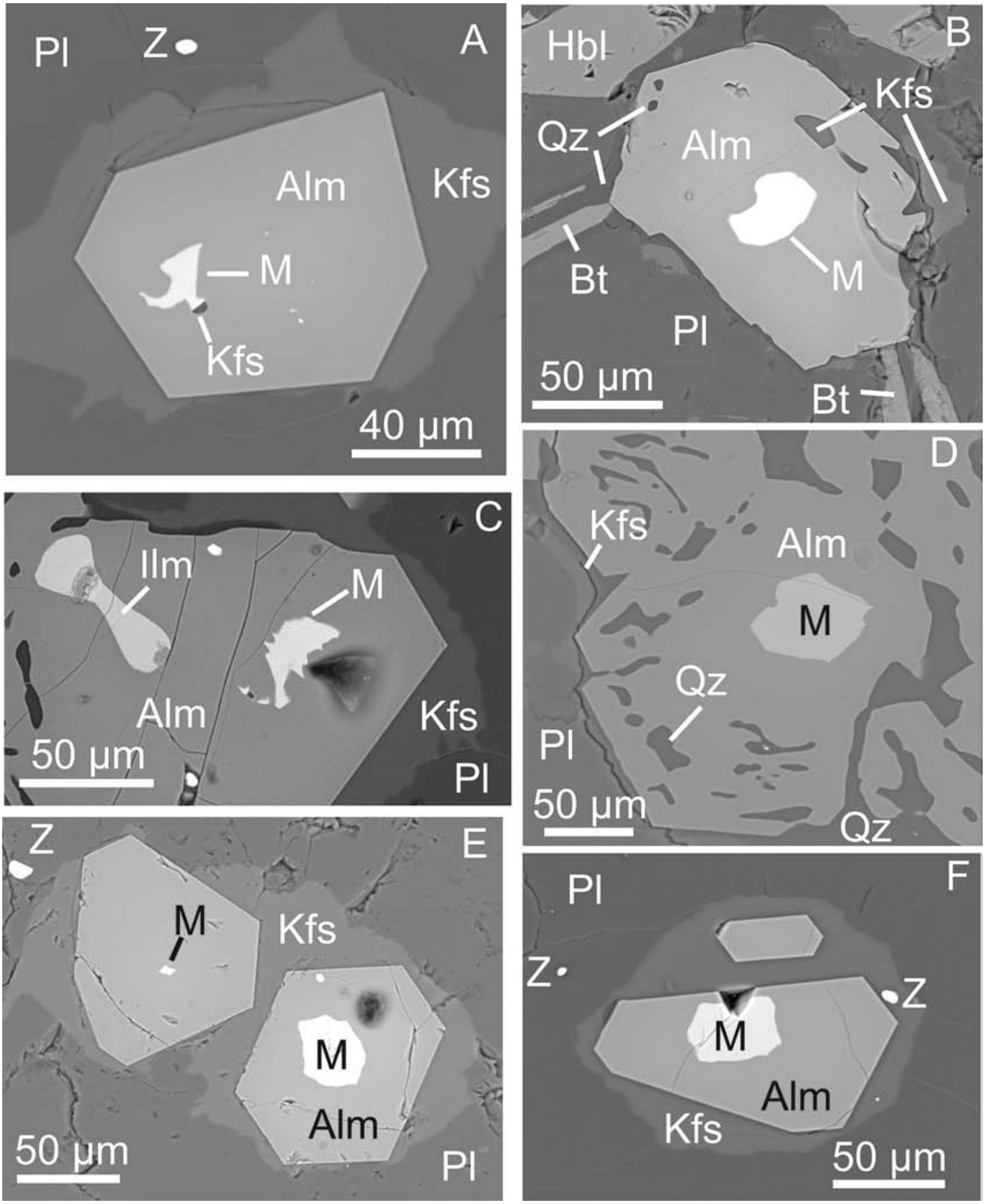

FIG. 4. Back-scattered electron images of menzerite-(Y). A. Sample GB50A2, grain #10. B. Sample GB94I4, grain 1. C. Sample GB50C, grain #7/1. D. Sample GB50A2, grain #1. E. Sample GB94I4B, grain #1. F. Sample GB50A2, grain #8. Abbreviations: Alm: almandine, Bt: biotite, Hbl: calcic amphibole, Ilm: ilmenite, Kfs: K-feldspar, M: menzerite-(Y), Pl: oligoclase, Qz: quartz, Z: zircon.

for menzerite-(Y) are 2.316 Å and 2.454 Å, respectively, which is within 0.01 Å with the refined distances (Table 4). Corresponding calculations were done for the *Y*–O distance in menzerite-(Y) with 16% Al, 28% Mg, 34% Fe^{3+}, and 22% Fe^{2+} (including minor transition metals) at the *Y* site. Reference distance-data for Mg and Fe^{2+} were taken from end-member forsterite and fayalite, Al from pyrope and almandine, and Fe^{3+} from andradite. The calculated distance is 2.056 Å, which is 0.03 Å longer than the refined value (Table 4). This discrepancy is consistent with the observation discussed in the section on Methods that site scattering at *Y* derived from EMPA is higher than the value obtained by site-occupancy refinement. This may indicate that strongly scattering ions with large radii in octahedral coordination are overestimated in the EMPA owing to chemical zoning or to the limitations of electron-beam size and penetration.

Owing to the presence of octahedral Mg and Fe^{2+}, menzerite-(Y) displays significantly longer *Y*–O distances, 2.0244(16) Å, compared to the associated almandine, 1.9132(17) Å (Table 4), which has Al dominant at the octahedral site.

We have no indication of Ti^{4+} or Fe in tetrahedral coordination based on the structural data of both almandine and menzerite-(Y). The population of silicon was not refined in order to reduce correlation problems with the scale factor. However, the refinement of the site occupancy of Mg and Fe at the *Y* site in menzerite-(Y) indicates esd values of *ca*. 1–2% (Table 2), and thus similar esd values would be expected for a Si *versus* Ti or Fe refinement. The similar and physically reasonable U_{eq} values for the tetrahedral sites (Table 3) do not point to any significant transition-metal concentration. Furthermore, the *Z*–O distances, 1.640 Å for almandine and 1.649 Å for menzerite-(Y) (Table 4), are characteristic of Si only at *Z* as in other garnets, *e.g.*, 1.628–1.645 Å for various Ca–Mg–Fe–Mn garnets (Novak & Gibbs 1971, Armbruster *et al*. 1992), 1.648–1.649 Å for synthetic andradite (Armbruster & Geiger 1993) *versus* 1.658–1.678 Å for andradite containing significant Ti or Fe at the *Z* site (Armbruster *et al*. 1998).

The Si–O distances and scattering power at *Z* are inconsistent with the presence of significant H_2O; *cf*. 1.762 Å, an average for hydrous andradite with 1.65 Si and 1.35 H_4O_4 per formula unit (Armbruster 1995).

Owing to the small grain-size, it was not possible to obtain a powder X-ray-diffraction pattern, so it was calculated for Cu$K\alpha_1$ radiation and Debye–Scherrer geometry from the single-crystal data using the LAZY PULVERIX software (Yvon *et al*. 1977) (Table 5).

MICRO-X-RAY ABSORPTION NEAR-EDGE SPECTROSCOPY AND Fe^{3+} CONTENT OF MENZERITE-(Y) AND ALMANDINE

The X-ray absorption spectra at the Fe *K*-edge were acquired at two points at the center of grain #5 on menzerite-(Y), and weighted peak-centers were calculated from the fits (Fig. 6). Our current calibration suggests that these correspond to $Fe^{3+}/\Sigma Fe$ values of 0.553 and 0.571, with errors estimated at ±0.05–0.1 absolute or better (work is still in progress to specifically determine the errors). Almandine at the edge of grain #5 was also analyzed twice, and yielded $Fe^{3+}/\Sigma Fe$ = 0.166 and 0.190, whereas almandine in grain #1 gave $Fe^{3+}/\Sigma Fe$ = 0.082 and 0.077. All analyses were made using thin section GB50A1.

Crystal-chemical formulae calculated from stoichiometry (see below) give $Fe^{3+}/\Sigma Fe$ in the range 0.37–0.50 for the 12 grains of menzerite-(Y). The calculated value for grain 5 (section 1, Table 6) is 0.39(2), with a 1σ error calculated by propagation using the spreadsheet modified from Locock (2008). This stoichiometric $Fe^{3+}/\Sigma Fe$ ratio is demonstrably lower than the micro-XANES $Fe^{3+}/\Sigma Fe$ = 0.56(10) for this grain. Similarly, the average stoichiometric $Fe^{3+}/\Sigma Fe \approx 0.05$ (Table 7) for the euhedral almandine is lower than the micro-XANES $Fe^{3+}/\Sigma Fe$ in the range 0.08–0.18(10) obtained on grains 1 and 5, but the discrepancy is less.

In summary, the micro-XANES $Fe^{3+}/\Sigma Fe$ values provide only partial confirmation of the $Fe^{3+}/\Sigma Fe$ values calculated by stoichiometry, and the discrepancy in the case of menzerite-(Y) raises the question as to whether we should use the micro-XANES results to calculate $Fe^{3+}/\Sigma Fe$ ratios for all the menzerite-(Y) grains. One difficulty is that interpretation of XANES data is not entirely straightforward in the presence of multiple coordination environments, as in the case for menzerite-(Y). Wilke *et al*. (2001), Berry *et al*. (2003) and Höfer *et al*. (2006) have cited the coordination of Fe as a complicating factor in determining $Fe^{3+}/\Sigma Fe$ using XANES data. Moreover, we have a micro-XANES determination on only one grain of menzerite-(Y) out of the 12 analyzed. Given the complexities in interpreting the micro-XANES $Fe^{3+}/\Sigma Fe$ values, we do not believe that it is appropriate to apply this one determination to the other 11 grains of menzerite because of compositional differences among them. Consequently, we have relied on the stoichiometric values of $Fe^{3+}/\Sigma Fe$ so that the results on the 12 grains would be directly comparable with one another. We have also relied on the stoichiometric values for almandine to maintain internal consistency.

CHEMICAL COMPOSITION OF MENZERITE-(Y) AND ALMANDINE

The salient compositional feature of menzerite-(Y) is its high content of Y and HREE, *e.g*., 13.03–16.93 wt% Y_2O_3 and 2.19–3.17 wt% Yb_2O_3 (Table 6), the highest by far reported in a natural garnet. We have based our calculation of the formula on the crystal-structure refinement as stated above, assuming full occupancy, 12 oxygen atoms and eight cations [method based on stoichiometry of Droop (1987), Giaramita & Day (1990)].

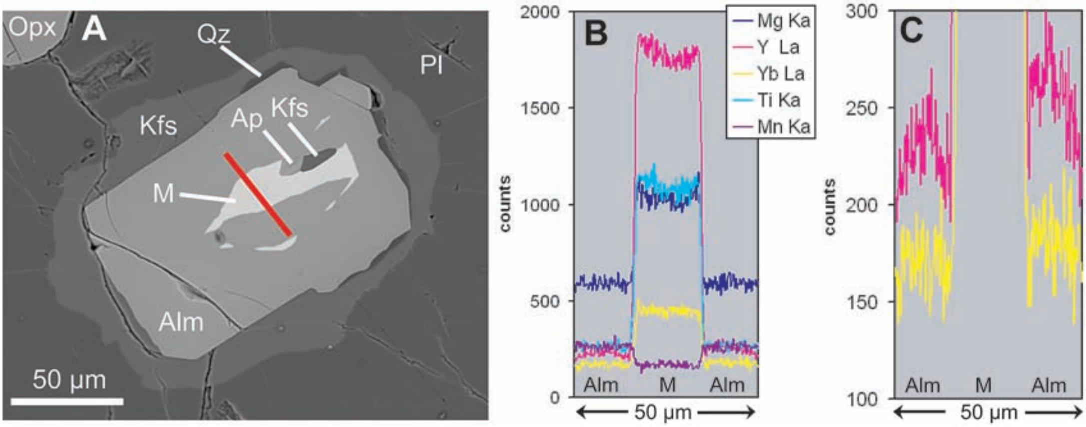

FIG. 5. Profile for selected constituents in menzerite-(Y) and enclosing almandine. A. Back-scattered electron image of sample GB50A1, grain #3, showing profile line (red). B. Profiles for five constituents along the 50 µm trace in A. C. Profiles for Y and Yb from B, but with ordinate (counts) expanded. Abbreviations: Alm: almandine, Ap: fluorapatite, Kfs: K-feldspar, M: menzerite-(Y), Opx: ferrosilite, Pl: oligoclase, Qz: quartz.

TABLE 4. BOND LENGTHS (Å) FOR MENZERITE-(Y) AND ALMANDINE

	Menzerite-(Y)	Almandine
$X-O^{\$}$	2.3272(17) × 4	2.2539(17) × 4
$X-O^{\#}$	2.4666(17) × 4	2.4135(17) × 4
$Y-O$	2.0244(16) × 6	1.9132(17) × 6
$Z-O$	1.6488(17) × 4	1.6403(17) × 4

$^{\$}$ O at –x, –y, –z + 1; x + 1/4, –z + 3/4, –y + 1/4; x + 1/4, z – 3/4, y + 1/4; –x, y, z – 1/2. $^{\#}$ O at z – 1/2, x, –y + 1/2; –z + 3/4, –y + 1/4, x + 1/4; –z + 3/4, y – 1/4, –x + 1/4; z – 1/2, –x, y.

We have also assumed that Cr and V are trivalent and Mn is divalent based on the following evidence, which is sufficient for our purposes, because these elements are present in such low concentrations in menzerite-(Y):

Cr: Geiger *et al.* (2000) reported only trivalent Cr in pyrope synthesized at 1050°C, 25 kbar; indeed, Cr is almost exclusively trivalent in metamorphic silicate minerals.

V: Geiger *et al.* (2000) reported tetravalent V in pyrope synthesized at 950–1050°C, 25 kbar, in one case with V metal to constrain oxygen fugacity, but found that the concentration of V^{3+} is "significantly higher" than that of V^{4+}.

Mn: At oxygen fugacities corresponding to 1–2 $\log_{10}$ units more oxidizing than the QFM buffer, Mn is expected to be predominantly divalent in menzerite-(Y), as it is in silicates and oxides synthesized at 600°C, 4 kbar at these oxygen fugacities (Abs-Wurmbach & Peters 1999).

TABLE 5. POWDER-DIFFRACTION PATTERN OF MENZERITE-(Y)

I (%)	$d_{calc.}$ (Å)	h	k	l	I (%)	$d_{calc.}$ (Å)	h	k	l
8	4.8968	2	1	1	1	1.6323	5	5	2
1	4.2408	2	2	0	1	1.6323	7	2	1
6	3.2057	3	2	1	44	1.6029	6	4	2
36	2.9987	4	0	0	1	1.5233	6	5	1
100	2.6821	4	2	0	10	1.4993	8	0	0
2	2.5573	3	3	2	1	1.4764	7	4	1
33	2.4484	4	2	2	9	1.3410	8	4	0
9	2.3524	4	3	1	18	1.3087	8	4	2
17	2.1899	5	2	1	1	1.2934	9	2	1
2	2.1204	4	4	0	1	1.2934	6	5	5
13	1.9458	5	3	2	7	1.2786	6	6	4
11	1.9458	6	1	1	1	1.2644	8	5	1
1	1.8965	6	2	0	1	1.2644	7	5	4
1	1.7685	6	3	1	1	1.2372	7	6	3
13	1.7313	4	4	4	1	1.2372	9	3	2
30	1.6634	6	4	0	1	1.2116	8	5	3
2	1.6323	6	3	3	1	1.2116	9	4	1

The pattern is calculated for Cu$K\alpha_1$ radiation and Debye–Scherrer geometry from the single-crystal data using LAZY PULVERIX (Yvon *et al.* 1977).

Although the precision of the averaged analytical results [standard deviations are given in Table 6 for the grain used to define menzerite-(Y)] justifies giving formula units only to the nearest 0.01 cations, we have tabulated cation proportions to the third decimal place so as to minimize accumulation of rounding-off errors.

In calculating a formula for menzerite-(Y) and identifying end-members, we follow Hatert & Burke (2008) in first considering the relative proportions of the cation valences at each of the three sites, then the relative proportion of cations for each valence at that site. The

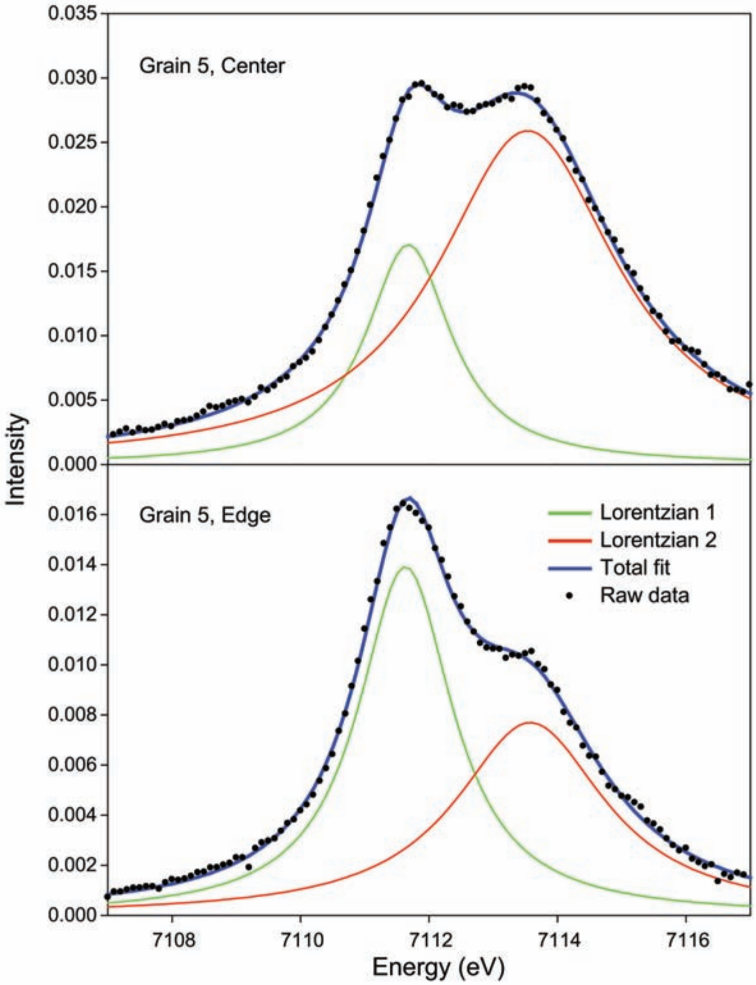

FIG. 6. Micro-XANES spectra of menzerite-(Y) in the center of grain 5 (top) contrasted with the edge of the grain, which is almandine. Both spectra have prominent peaks at *ca*. 7111.6 eV and 7113.5 eV, but the areas are dramatically different, giving rise to weighted positions of 7113.1 eV for menzerite-(Y) and 7112.6 eV for almandine.

Z site is dominated by the tetravalent cation, Si. The *Y* site is dominated by divalent cations in grains #5 and #6 (section GB50A1) and by trivalent cations in the other 10 grains (Fig. 7a). Of the two divalent cations, Mg exceeds Fe^{2+} in all the analyzed grains, whereas Fe^{3+} is the dominant trivalent cation in these grains. The *X* site is dominated by divalent cations with Ca > (Fe^{2+} + Mn^{2+}) in all the analyzed grains (Fig. 7b).

These observations suggest that menzerite-(Y) consists largely of two end-members, $\{Y_2Ca\}[Mg_2](Si_3)O_{12}$, which has not been reported previously, and andradite, $\{Ca_3\}[Fe^{3+}_2](Si_3)O_{12}$, where {}, [] and () enclose occupants at the *X*, *Y* and *Z* sites, respectively, as recommended by Geller (1967). Because charge balance allows only 2Y at *X* for Si = 3 at *Z*, we have drawn the boundary in Figure 7b between $\{Y_2Ca\}[Mg_2](Si_3)O_{12}$ and $\{Ca_3\}[Fe^{3+}_2](Si_3)O_{12}$ at 0.333 instead of 0.5. Thus, grains #5 and #6 plot in the field where the $\{Y_2Ca\}[Mg_2](Si_3)O_{12}$ end-member is dominant. Moreover, Mg/(Mg + Fe^{2+}) covers the range 0.54–0.66 at the *Y* site, implying an important role for the end-member $\{Y_2Ca\}[Fe^{2+}_2](Si_3)O_{12}$, whereas the presence of Al at the *Y* site and Fe^{2+} at the *X* site implies a role for almandine in addition to andradite. As the compositions of the grains plot close to the boundaries between the end members $\{Y_2Ca\}[Mg_2](Si_3)O_{12}$ and $\{Y_2Ca\}[Fe^{2+}_2]$

TABLE 6. COMPOSITIONS OF MENZERITE-(Y) IN SECTIONS GB50A1 AND GB50A2

Section-grain # of points	1-1* 10	1-2# 10	1-3 9	1-5§ 10	1-6 10	2-1 10	2-2 9	2-3 10	2-4 10	2-5 10	2-8 9	2-9 9
SiO_2 wt%	30.38	30.62	30.33	30.64 (0.18)	30.14	31.00	29.65	30.08	30.77	31.35	30.67	30.13
TiO_2	1.38	1.46	0.86	1.10 (0.06)	2.66	1.04	1.27	1.56	1.32	0.95	1.32	1.33
Al_2O_3	4.46	4.08	4.43	4.87 (0.25)	3.32	4.73	4.72	3.93	4.47	5.05	4.96	4.29
Sc_2O_3	0.32	0.29	0.15	0.17 (0.01)	0.13	0.06	0.21	0.19	0.32	0.17	0.20	0.16
V_2O_3	0.33	0.36	0.32	0.17 (0.03)	0.24	0.27	0.42	0.32	0.59	0.32	0.54	0.37
Cr_2O_3	0.15	–	0.17	0.04 (0.02)	0.15	0.13	0.27	0.18	0.18	0.21	0.17	0.12
Fe_2O_3	10.77	9.51	9.60	8.38†	8.48	11.97	10.91	10.99	10.35	7.76	10.13	11.05
FeO	9.97	11.35	10.19	11.82†	10.77	10.70	9.71	9.81	10.50	11.83	11.04	10.29
MnO	0.96	0.42	0.95	0.85 (0.07)	0.76	0.77	1.07	1.03	1.14	1.32	1.29	0.98
MgO	3.85	3.99	4.16	3.98 (0.08)	4.00	3.60	3.90	3.75	3.61	4.09	3.68	3.72
CaO	15.42	14.87	14.42	13.92 (0.11)	15.43	15.70	14.71	15.48	15.53	13.97	14.80	15.08
Y_2O_3	14.42	13.11	15.42	16.93 (0.38)	15.33	13.03	14.56	14.31	14.17	15.16	13.77	14.44
La_2O_3	0.00	0.00	0.09	0.00 (0.01)	0.02	0.00	0.00	0.00	0.00	0.01	0.00	0.00
Ce_2O_3	0.01	0.00	0.08	0.01 (0.02)	0.07	0.02	0.06	0.06	0.02	0.00	0.02	0.02
Pr_2O_3	0.01	0.00	0.12	0.00 (0.02)	0.04	0.02	0.00	0.00	0.00	0.00	0.02	0.06
Nd_2O_3	0.11	0.18	0.18	0.12 (0.02)	0.20	0.09	0.10	0.15	0.14	0.03	0.10	0.12
Sm_2O_3	0.22	0.12	0.47	0.15 (0.05)	0.44	0.22	0.23	0.19	0.22	0.09	0.18	0.19
Eu_2O_3	0.05	0.00	0.12	0.01 (0.02)	0.02	0.04	0.05	0.06	0.06	0.05	0.08	0.07
Gd_2O_3	0.22	0.39	0.54	0.36 (0.02)	0.64	0.29	0.40	0.49	0.33	0.30	0.41	0.33
Tb_2O_3	0.03	0.07	0.19	0.11 (0.02)	0.13	0.08	0.08	0.08	0.08	0.06	0.09	0.08
Dy_2O_3	0.91	1.40	1.74	1.52 (0.05)	1.47	0.91	1.00	1.02	1.10	0.99	1.10	0.90
Ho_2O_3	0.46	0.46	0.91	0.63 (0.04)	0.61	0.50	0.58	0.58	0.53	0.53	0.50	0.52
Er_2O_3	2.25	2.45	2.69	2.40 (0.05)	2.62	2.25	2.50	2.55	2.14	2.57	2.25	2.57
Tm_2O_3	0.43	0.09	0.63	0.38 (0.02)	0.48	0.48	0.49	0.49	0.42	0.50	0.43	0.54
Yb_2O_3	2.62	2.19	3.17	2.03 (0.06)	2.52	2.75	2.83	2.87	2.38	3.06	2.48	2.95
Lu_2O_3	0.83	0.00	1.55	0.68 (0.05)	0.83	1.02	0.92	0.83	0.85	0.95	0.80	1.00
Sum	100.57	97.40	103.50	101.26	101.48	101.67	100.66	101.00	101.23	101.34	101.03	101.32
Si *apfu*	2.791	2.874	2.786	2.820	2.792	2.813	2.747	2.781	2.809	2.869	2.804	2.777
^{Z}Al	0.209	0.126	0.214	0.180	0.208	0.187	0.253	0.219	0.191	0.131	0.196	0.223
Ti	0.095	0.103	0.060	0.076	0.185	0.071	0.088	0.108	0.091	0.066	0.091	0.092
^{Y}Al	0.274	0.326	0.266	0.348	0.155	0.319	0.262	0.209	0.291	0.413	0.338	0.244
Fe^{3+}	0.745	0.672	0.664	0.580	0.591	0.817	0.761	0.765	0.711	0.534	0.697	0.766
Sc	0.026	0.023	0.012	0.013	0.010	0.005	0.017	0.016	0.025	0.013	0.016	0.013
V	0.025	0.027	0.024	0.013	0.018	0.020	0.031	0.024	0.043	0.024	0.039	0.027
Cr	0.011	–	0.012	0.003	0.011	0.010	0.020	0.013	0.013	0.015	0.012	0.009
Mg	0.528	0.558	0.570	0.546	0.552	0.486	0.538	0.517	0.492	0.557	0.501	0.511
$^{Y}Fe^{2+}$	0.297	0.291	0.393	0.421	0.477	0.272	0.283	0.348	0.334	0.377	0.306	0.338
Sum *Y*	2.000	2.000	2.000	2.000	2.000	2.000	2.000	2.000	2.000	2.000	2.000	2.000
Y + REE	0.939	0.872	1.117	1.072	1.051	0.875	0.987	0.976	0.926	1.000	0.913	0.979
Ca	1.517	1.495	1.420	1.373	1.532	1.526	1.460	1.533	1.519	1.370	1.450	1.489
Mn	0.075	0.034	0.074	0.066	0.059	0.059	0.084	0.081	0.088	0.102	0.100	0.077
$^{X}Fe^{2+}$	0.469	0.599	0.390	0.489	0.358	0.540	0.469	0.410	0.467	0.528	0.538	0.455
Sum *X*	3.000	3.000	3.000	3.000	3.000	3.000	3.000	3.000	3.000	3.000	3.000	3.000
Sum R^{2+} at *Y*	0.825	0.849	0.962	0.967	1.029	0.759	0.822	0.865	0.826	0.935	0.807	0.848
Sum R^{3+} at *Y*	1.080	1.047	0.978	0.957	0.786	1.170	1.090	1.026	1.084	1.000	1.102	1.059
Sum R^{4+} at *Y*	0.095	0.103	0.060	0.076	0.185	0.071	0.088	0.108	0.091	0.066	0.091	0.092
Sum at *Y*	2.000	2.000	2.000	2.000	2.000	2.000	2.000	2.000	2.000	2.000	2.000	2.000
$Fe^{3+}/\Sigma Fe$	0.49	0.43	0.46	0.39	0.41	0.50	0.50	0.50	0.47	0.37	0.45	0.49

Note: both F and Na were sought in WDS scans, but not detected. The amounts of FeO and Fe_2O_3 were calculated from total Fe measured as FeO and the Fe^{2+}/Fe^{3+} ratio in the formulae. Standard deviations are in round brackets. * Grain used to measure *n*. # Grain used for structure refinement; analyzed by a different protocol (see text). § Grain used to define menzerite-(Y). † Fe measured as FeO = 19.36 (0.15) wt.%. The compositions were acquired with an electron microprobe; the formulae are based on eight cations and twelve atoms of oxygen.

$(Si_3)O_{12}$ on the one hand, and $\{(Ca,Fe)_3\}[(Fe^{3+},Al)_2](Si_3)O_{12}$ on the other (Fig. 7), the general formula for these grains contains both the Y-bearing and Y-free end-members, that is, $\{(Y,REE)(Ca,Fe^{2+})_2\}[(Mg,Fe^{2+})(Fe^{3+},Al)](Si_3)O_{12}$. Zoning in menzerite-(Y) grains can be interpreted as variations in the relative proportions of the two end-members $\{Y_2Ca\}[(Mg,Fe^{2+})_2](Si_3)O_{12}$ considered together and $\{(Ca,Fe)_3\}[(Fe^{3+},Al)_2](Si_3)O_{12}$ in which the proportion of the Yb analogue of $\{Y_2Ca\}[(Mg,Fe^{2+})_2](Si_3)O_{12}$ remains relatively constant (Figs. 3, 5b).

An alternative approach to calculate end-members was advocated by Rickwood (1968), because in contrast to most silicate minerals, garnet end-member proportions constitute an under-determined system from the point of view of linear algebra. As presently constituted (*e.g.*, Back & Mandarino 2008), there are more end-members in the garnet group than oxides, resulting in ambiguity. Rickwood (1968) emphasized that the sequence of calculation influences the results, and therefore recommended that all investigators use the same sequence so that their results would be comparable. Locock (2008) expanded Rickwood's work to include almost all components present in natural garnet. Of the possible Y-bearing components, only $\{Y_3\}[Al_2](Al_3)O_{12}$ was included. With the discovery of menzerite-(Y), the

TABLE 7. REPRESENTATIVE COMPOSITIONS OF ALMANDINE

Section GB-	50A1	50A1	50A1	50A1	50A1	50C	50C	94I4	94I4
grain	1a2	1b2	2a2	3b2*	2b2	6-2	1-2	1c	2a
Type	Euh	Euh	Euh	Euh	Sym	Sym	Sym	w/Bt	w/Bt
# of points	8	4	5	3	10	7	10	10	7
SiO_2 wt%	36.78	36.94	37.37	36.87	37.63	37.43	37.23	37.16	37.32
TiO_2	0.05	0.03	0.12	0.06	0.01	0.16	0.13	0.03	0.03
Al_2O_3	18.79	19.14	19.62	19.71	20.62	20.35	20.15	20.14	20.20
V_2O_3	0.12	0.08	0.07	0.08	0.04	–	–	–	–
Cr_2O_3	0.11	0.09	0.05	0.02	0.00	–	–	–	–
Fe_2O_3	1.44	1.20	1.52	1.42	1.07	0.60	0.82	1.77	1.92
FeO	25.84	25.99	27.98	26.74	30.13	30.01	29.78	29.05	29.03
MnO	1.80	1.83	1.68	1.71	1.34	1.55	1.51	2.32	2.25
MgO	2.80	2.75	2.55	2.76	2.44	2.63	2.57	2.48	2.63
CaO	8.89	8.94	8.25	8.39	7.15	6.72	6.82	6.75	6.75
Y_2O_3	1.72	1.58	0.60	1.12	0.17	0.04	0.14	0.09	0.00
Gd_2O_3	0.12	0.11	0.00	0.12	0.00	–	–	–	–
Dy_2O_3	0.01	0.04	0.00	0.00	0.00	–	–	–	–
Er_2O_3	0.43	0.39	0.23	0.30	0.10	–	–	–	–
Yb_2O_3	0.68	0.58	0.27	0.33	0.04	–	–	–	–
Na_2O	–	–	–	–	–	0.01	0.00	0.00	0.00
K_2O	–	–	–	–	–	0.00	0.00	0.00	0.01
Sum	99.57	99.67	100.31	99.62	100.76	99.48	99.16	99.77	100.14
Si *apfu*	2.992	2.994	2.997	2.979	2.994	3.008	3.006	2.988	2.988
^{Z}Al	0.008	0.006	0.003	0.021	0.006	0.000	0.000	0.012	0.012
Ti	0.003	0.002	0.007	0.003	0.001	0.010	0.008	0.002	0.002
^{Y}Al	1.793	1.822	1.851	1.855	1.927	1.928	1.918	1.897	1.893
Fe^{3+}	0.088	0.073	0.092	0.086	0.064	0.036	0.050	0.107	0.116
V	0.008	0.005	0.004	0.005	0.003	–	–	–	–
Cr	0.007	0.006	0.003	0.001	0.000	–	–	–	–
^{Y}Mg	0.101	0.092	0.042	0.049	0.005	0.026	0.025	0.000	0.000
Sum *Y*	2.000	2.000	2.000	2.000	2.000	2.000	2.000	2.006	2.011
Y + REE	0.106	0.096	0.038	0.067	0.011	0.002	0.006	0.004	0.000
Ca	0.774	0.776	0.709	0.726	0.610	0.578	0.590	0.581	0.579
Mn	0.124	0.125	0.114	0.117	0.091	0.105	0.103	0.158	0.152
$^{X}Fe^{2+}$	1.758	1.762	1.876	1.806	2.005	2.017	2.011	1.954	1.943
^{X}Mg	0.238	0.240	0.263	0.284	0.284	0.288	0.284	0.297	0.314
Na	–	–	–	–	–	0.001	0.000	0.000	0.000
K	–	–	–	–	–	0.000	0.000	0.000	0.001
Sum *X*	3.000	3.000	3.000	3.000	3.000	2.992	2.994	2.994	2.989
Total cations	8.000	8.000	8.000	8.000	8.000	8.000	8.000	8.000	8.000
$Fe^{3+}/\Sigma Fe$	0.048	0.040	0.047	0.046	0.031	0.018	0.024	0.052	0.056

Note: the amounts of FeO and Fe_2O_3 were calculated from stoichiometry. ^{Y}Mg is calculated to bring occupancy of the *Y* site to 2 unless $Y > 2$ *apfu*. Microstructure type: Euh: euhedral, Sym: symplectite with quartz ± augite, w/Bt: symplectite with biotite. * Grain used for structure refinement (Table 2). The compositions were acquired with an electron microprobe; the formulae are based on eight cations and twelve atoms of oxygen.

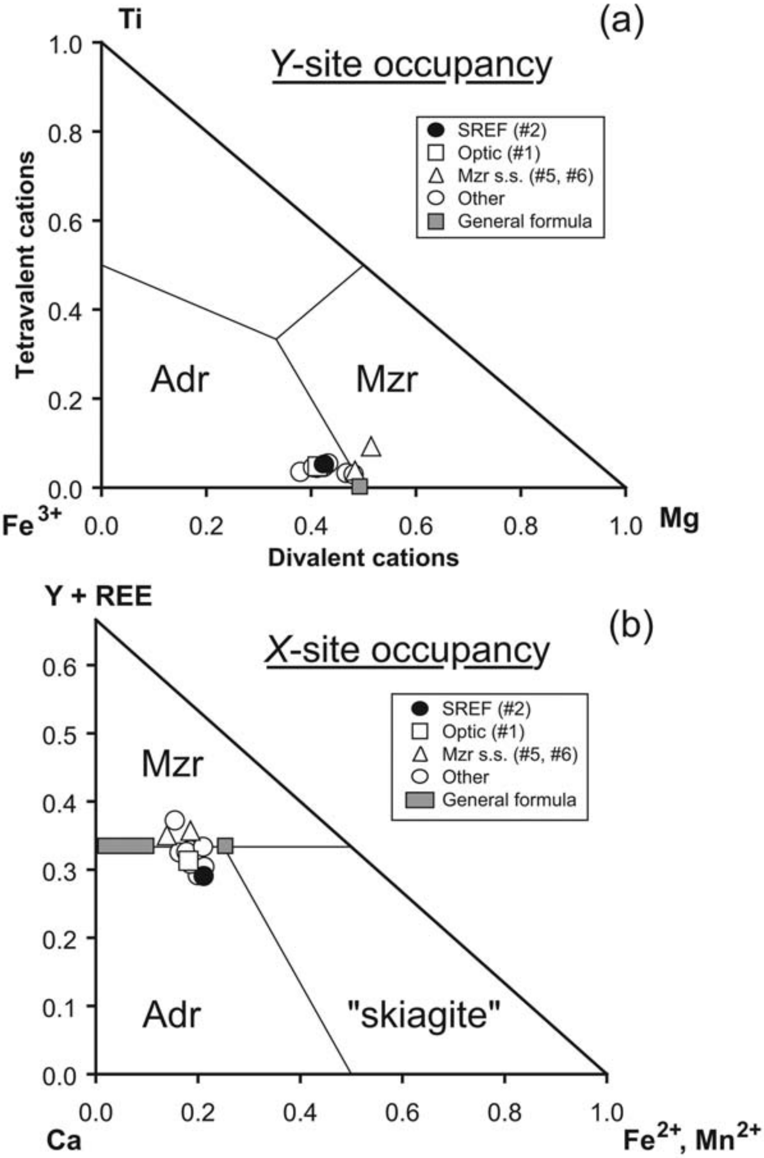

FIG. 7. Plot of menzerite-(Y) compositions in terms of site occupancy and cation valence (mole proportions). Numbers refer to grains in section GB50A1 used for the crystal-structure refinement (SREF), optical measurements, and menzerite-(Y) *sensu stricto*, including grain #5 used as the holotype to characterize the mineral. Open circles indicate the other nine grains analyzed in sections GB50A1 and GB50A2 (Table 6). The general formula refers to $\{(Y,REE)(Ca,Fe^{2+})_2\}[(Mg,Fe^{2+})(Fe^{3+},Al)](Si_3)O_{12}$. (a) The corners are labeled by the dominant cation for a given valence at the *Y* site in menzerite-(Y). No mineral is specified for the Ti field because of the complex substitutions in Ti-rich garnets. (b) The divalent cations are split into Ca-dominant and Fe^{2+}-dominant fields. The Y+REE occupancy cannot exceed $^2/_3$ owing to charge-balance considerations unless Si < 3 *apfu*. The general formula applies to the entire length of the boundary between andradite and menzerite-(Y), but is split in two so as to not obscure the data points.

spreadsheet had to be modified to include the $\{Y_2Ca\}[Mg_2]Si_3O_{12}$ (menzerite) and its Fe^{2+} analogue $\{Y_2Ca\}[Fe^{2+}{}_2]Si_3O_{12}$ ("menzerite-Fe") end-members, both meeting the attributes of a valid end-member formula (Hawthorne 2002). For calculating the proportion of Y-bearing components, the REE were added to Y. Menzerite is dominant in recalculated compositions of 10 of the 12 grains analyzed, and andradite is dominant in the other two (Table 8). Overall, the end-members andradite, almandine, $\{Y_2Ca\}[Mg_2]Si_3O_{12}$ [menzerite-(Y)], $\{Y_2Ca\}[Fe^{2+}{}_2]Si_3O_{12}$, and $\{Fe^{2+}{}_3\}[Fe^{3+}{}_2]Si_3O_{12}$ ("skiagite") compose 71–83% of the analyzed grains, with morimotoite and "yttrogarnet" being the most abundant components in the remainder.

The composition of menzerite-(Y) varies from grain to grain, but the only regular variations with Y + REE are the increase in Mg (Fig. 8) and the decrease in total trivalent cations. In addition, individual grains are zoned, commonly with Mg, Ti, Y and Er (to a lesser extent) increasing toward the rim, but with Al and Ca decreasing and Yb remaining relatively constant (*e.g.*, Figs. 3, 5b). Both grain-to-grain variation and zonation of individual grains are best understood in terms of variation of Fe-bearing menzerite-(Y), $\{Y_2Ca\}[(Mg,$

TABLE 8. COMPOSITION OF MENZERITE-(Y) IN TERMS OF GARNET END-MEMBERS

Section-grain	1-1*	1-2[#]	1-3	1-5[§]	1-6	2-1	2-2	2-3	2-4	2-5	2-8	2-9
Yttrogarnet	6.98	4.20	7.13	6.01	6.92	6.24	8.45	7.30	6.36	4.37	6.55	7.43
Menzerite	26.38	27.90	28.48	27.32	27.60	24.32	26.91	25.84	24.59	27.87	25.06	25.53
Menzerite-Fe	10.09	9.41	16.66	17.25	14.58	10.09	9.74	12.00	12.16	15.58	10.76	12.26
Morimotoite	9.53	10.33	5.97	7.59	18.53	7.07	8.84	10.85	9.07	6.57	9.11	9.25
Sc garnet**	1.29	1.17	0.60	0.66	0.51	0.25	0.83	0.78	1.27	0.66	0.78	0.65
Goldmanite	1.23	1.34	1.19	0.63	0.90	0.98	1.55	1.18	2.17	1.18	1.97	1.35
Uvarovite	0.55		0.61	0.14	0.56	0.48	1.01	0.64	0.66	0.75	0.61	0.46
Spessartine	2.50	1.12	2.45	2.21	0.84	1.97	2.81	2.70	2.94	3.40	3.33	2.56
Almandine	4.22	10.95	3.72	9.18		7.73	1.82	0.48	5.23	12.90	7.01	2.19
Andradite	25.81	24.56	23.91	21.88	16.50	30.61	24.22	25.03	25.20	22.01	23.92	25.33
Calderite					1.15							
Skiagite	11.41	9.02	9.28	7.12	11.92	10.25	13.81	13.20	10.35	4.70	10.92	12.99
Remainder	0.00	0.00	0.00	0.00	0.00	0.00	0.00	0.00	0.00	0.00	0.00	0.00
Sum	99.99	100.00	100.00	99.99	100.01	99.99	99.99	100.00	100.00	99.99	100.02	100.00

Note: * Grain used to measure *n*. [#] Grain used for structure refinement; analyzed by a different protocol (see text). [§] Grain used to define menzerite-(Y). ** Eringaite. All compositions gave a superior quality index. Mineral names are listed in regular font, hypothetical end-members are in italics. The proportion of end members, expressed in mole %, was calculated from a spreadsheet adapted from Locock (2008).

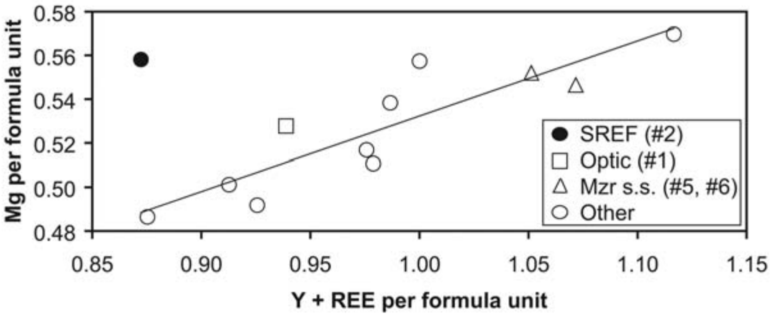

FIG. 8. Plot of Mg *versus* sum of Y + REE in menzerite-(Y). Numbers refer to grains in sections GB50A1 used for the crystal-structure refinement (SREF), optical measurements, and menzerite-(Y) *sensu stricto*, including grain #5 used as the holotype to characterize the mineral (Table 6). A least-squares fit to all the points except SREF (grain #2), which was analyzed under different conditions, gives Mg = 0.34 (Y + REE) + 0.19, R^2 = 0.79.

$Fe^{2+})_2]Si_3O_{12}$, *versus* andradite–grossular, $\{(Ca, Fe)_3\}[(Fe^{3+},Al)_2](Si_3)O_{12}$.

Euhedral grains of almandine, including several overgrowing menzerite-(Y), contain up to 2.7 wt% Y_2O_3 (at one analytical point; in most cases, analyzed areas contain less than 1.8 wt% Y_2O_3) and up to 0.68 wt% Yb_2O_3 (*e.g.*, Table 7), the contents of which increase from rim to core, except for a dip in Y content next to the contact with menzerite-(Y) in some grains (Fig. 5c). Incorporation of Y and REE appears to be largely through incorporation of menzerite-(Y) and its Fe^{2+} analogue rather than through incorporation of the "yttrogarnet" component (YAG), $\{Y_3\}[Al_2](Al_3)O_{12}$, and its Fe^{3+} analogue, YIG, $\{Y_3\}[Fe^{3+}{}_2](Fe^{3+}{}_3)O_{12}$

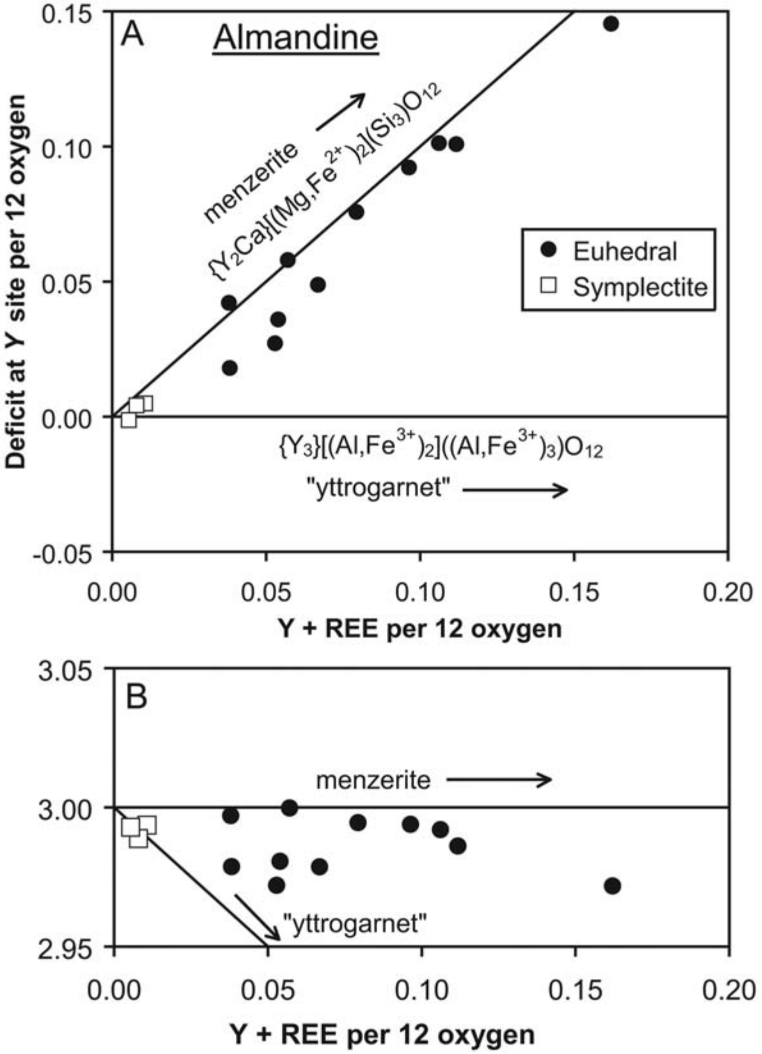

FIG. 9. Plot of compositions of almandine associated with menzerite-(Y) in sample GB50A (section 1). The plotted data are averages of 3 to 10 analyses (*e.g.*, Table 7), except for the point richest in Y (one analysis). Euhedral: isolated euhedral almandine grains, in some cases surrounding menzerite-(Y); symplectite: symplectite of almandine with vermicules of quartz . The generalized components $\{Y_2Ca\}[(Mg,Fe^{2+})_2](Si_3)O_{12}$ and $\{Y_3\}[(Al,Fe^{3+})_2]((Al,Fe^{3+})_3)O_{12}$, are the menzerite and "yttrogarnet" substitutions, respectively. A. Plot of the deficit at the *Y* site, equal to 2 – [Ti + V + Cr + Sc + (Al – ^{Z}Al)], *versus* total Y + REE per formula unit of eight cations and 12 atoms of oxygen. B. Plot of Si *versus* total Y + REE, using the same formula basis.

(Fig. 9). That is, Ti + V + Cr + (Al – ^{Z}Al) decreases to 1.855 and Y + REE + Fe^{2+} + Mn + Mg + Ca reaches 3.145 atoms per 12 O, suggesting that the *Y* site is not fully occupied by trivalent cations and Ti, whereas the *X* site is overfilled with divalent cations. The higher Ca content in the euhedral almandine compared to other almandine (Fig. 10) is consistent with incorporation of menzerite. Because the *X* site is dominantly occupied by Fe^{2+} in almandine, addition of the menzerite components should increase the Ca content at a ratio of Ca to (Y + REE) = 0.5. The calcium content increases linearly with Y + REE content, but the measured ratio is 1.035 (Fig. 10), possibly due to addition of andradite concomitantly with menzerite. Direct measurement by micro-XANES confirms the stoichiometric calculations showing that Fe^{3+}/ΣFe is significantly lower in almandine than in associated menzerite-(Y). The dominant components in the euhedral almandine are almandine, grossular and pyrope, and the proportion of menzerite reaches 6.7%, whereas "yttrogarnet" does not exceed 1% (*e.g.*, Table 9).

In contrast, the Y and HREE contents of almandine in symplectites with quartz and augite or with biotite and quartz are close to the detection limit on the electron microprobe; the Ca contents of this almandine are sensibly lower (Fig. 10). Nonetheless, grossular is still the second most abundant component (Table 9).

DEFINITION OF MENZERITE-(Y) AND ITS RELATIONSHIP TO OTHER SPECIES OF GARNET

Following the dominant valence rule (Hatert & Burke 2008), menzerite-(Y) is defined as a garnet rich in Y and HREE in which divalent cations are dominant at the *Y* site, Mg is the dominant divalent cation at this site, and Y is dominant among Y + REE. Majorite is the only other natural garnet species in which divalent cations are dominant at the *Y* site, but it is distinct from menzerite-(Y) in that Y contents are negligible, and significant Si occupies the *Y* site (*e.g.*, Smith & Mason 1970, Mao *et al.* 1982). The end-member for menzerite-(Y) is $\{Y_2Ca\}[Mg_2](Si_3)O_{12}$; its Fe^{2+} analogue would be $\{Y_2Ca\}[Fe^{2+}{}_2](Si_3)O_{12}$, which has not yet been found.

However, the 12 Y-rich garnet grains analyzed in this study are intermediate in composition between menzerite-(Y) plus its Fe^{2+} analogue on the one hand, and andradite plus a "skiagite" component on the other, *i.e.*, close to the formula, $\{(Y, REE)(Ca, Fe^{2+})_2\}[(Mg,Fe^{2+})(Fe^{3+},Al)](Si_3)O_{12}$. Only two of the analyzed grains, namely #5 and #6, qualify as menzerite-(Y) under this definition, and even their compositions plot close to the boundary with andradite [menzerite-(Y) *sensu stricto* in Fig. 7]. The other 10, including those used for single-crystal X-ray diffraction and optical characterization, are, strictly speaking, andradite that is rich in the menzerite-(Y) component plus its Fe^{2+} analogue (Fig. 7). Grains of menzerite-(Y) *sensu stricto* are indistinguishable from Y-rich andradite in thin section and back-scattered electron images, and can only be identified with a complete, quantitative chemical analysis. Consequently, all grains similar to menzerite-(Y) *sensu stricto* in composition, optical appearance or electron scattering intensity are referred to menzerite-(Y) in the present paper.

The coupled substitutions $^{X}Y + {}^{Y}Mg = {}^{X}Ca + {}^{Y}Al$ and $^{X}Y + {}^{Y}Mg = {}^{X}Ca + {}^{Y}Fe^{3+}$ relate menzerite-(Y) to gros-

TABLE 9. COMPOSITION OF ALMANDINE IN TERMS OF GARNET END-MEMBERS

Section GB-	50A1	50A1	50A1	50A1	50A1	50C	50C	94I4	94I4
grain	1a2	1b2	2a2	3b2	2b2	6-2	1-2	1c	2a
Type	Euh	Euh	Euh	Euh	Sym	Sym	Sym	w/Bt	w/Bt
Yttrogarnet	0.27	0.20	0.10	0.71	0.21			0.13	0.01
Menzerite	4.91	4.51	1.75	2.27	0.21	0.08	0.31		
Schorlomite-Al								0.10	0.09
NaTi garnet						0.06			
Morimotoite-Mg	0.31	0.19	0.72	0.34	0.06	0.85	0.78		
Majorite						0.80	0.56		
Goldmanite	0.38	0.27	0.21	0.27	0.14				
Uvarovite	0.36	0.28	0.17	0.06					
Spessartine	4.12	4.18	3.80	3.91	3.02	3.52	3.45	5.26	5.08
Pyrope	7.93	8.02	8.77	9.45	9.48	9.08	9.10	9.91	10.45
Almandine	58.59	58.72	62.55	60.21	66.82	67.23	67.02	65.13	64.78
Grossular	18.74	19.98	17.35	18.46	16.83	16.56	16.31	14.44	14.33
Andradite	4.39	3.65	4.58	4.32	3.22	1.82	2.48	4.84	4.88
Remainder	0.00	0.00	0.00	0.00	0.00	0.00	0.00	0.20	0.38
Total	100.00	100.00	100.00	100.00	99.99	100.00	100.01	100.01	100.00

Note: All compositions gave a superior quality index. Mineral names are listed in regular font, hypothetical end-members are in italics. The proportion of end members, expressed in mole %, was calculated from a spreadsheet adapted from Locock (2008). K has been converted to the Na equivalent. Microstructure type: Euh: euhedral, Sym: symplectite with quartz ± augite, w/Bt: symplectite with biotite.

sular and andradite, respectively, whereas homovalent substitutions, *i.e.*, Mg = Ca and Fe = Ca at the *X* site, are required to relate it to pyrope and almandine. Previous investigators found Y and REE to be incorporated in various garnets through the coupled substitutions ^{X}Y + ^{Z}Al = ^{X}Mn + ^{Z}Si, ^{X}Y + ^{Z}(Fe^{3+},Al) = ^{X}Ca + ^{Z}Si or Na + Y = 2(Ca,Mn) at the *X* site (Jaffe 1951, Yoder & Keith 1951, Kasowski & Hogarth 1968, Enami *et al.* 1995, Røhr *et al.* 2007). In contrast, Wang *et al.* (2003a, 2003b) suggested the substitution (Y, REE) = Al to explain compositional variations in Y-bearing spessartine from the Xihuashan granitic complex, China. Our plot of these spessartine compositions (E.S. Grew, unpubl. data) suggests an alternative explanation for the inverse relation between Y+REE and Al: ^{X}Y + ^{Y}Fe^{2+} = ^{X}Mn + ^{Y}Al, *i.e.*, incorporation of the Fe^{2+} analogue of menzerite-(Y), $\{Y_2Ca\}[Fe^{2+}_2](Si_3)O_{12}$.

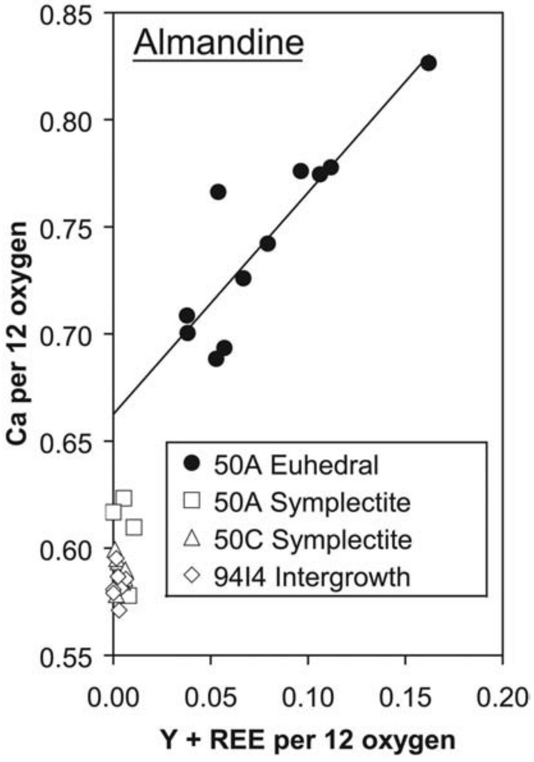

FIG. 10. The Ca and Y + REE contents in almandine associated with menzerite-(Y) in samples GB50A, GB50C and GBI4. The plotted data are averages of three to 10 analyses (*e.g.*, Table 7), except for the point richest in Y (one analysis). Euhedral: isolated euhedral almandine grains, in some cases surrounding menzerite-(Y), Symplectite: symplectite of almandine with vermicules of quartz ± augite, Intergrowth: symplectite of almandine with planar inclusions of quartz and overgrown by platelets of biotite. Line is a least-squares fit to the data for euhedral almandine: Ca = 1.035(Y + REE) + 0.663, $R^2 = 0.784$.

We are not aware of either end-member $\{Y_2Ca\}[Mg_2](Si_3)O_{12}$ or $\{Y_2Ca\}[Fe^{2+}_2](Si_3)O_{12}$ having been synthesized, although several Y–Mg–Al garnets lacking Ca have been (Ito 1967, Suwa *et al.* 1970, 1971). Reinen (1964) reported the synthesis of a Ge analogue of menzerite-(Y), $\{Y_2Ca\}[Mg_2]Ge_3O_{12}$, whereas Setlur *et al.* (2006) synthesized a garnet approaching the Lu analogue, with the nominal composition $\{Lu_2Ca\}[Mg_2]Si_3O_{12}$ and *a* = 11.9758(3) Å, but a Rietveld refinement gave the Lu:Ca ratio as 1.5:1.

CONDITIONS OF FORMATION AND ORIGIN OF MENZERITE-(Y)

Microstructures suggest that menzerite-(Y) is an early-formed mineral that was subsequently preserved by being armored by almandine and K-feldspar. Although menzerite-(Y) is no longer in contact with oligoclase, quartz, ferrosilite, magnetite and ilmenite, we presume that menzerite-(Y) was originally stable with these phases. Menzerite-(Y) was probably also stable with augite, even though it has not been found in the patches where coarse-grained, presumably primary augite is present. However, euhedral Y-bearing almandine, with a K-feldspar moat, does occur in such a patch; we suggest that this almandine marks the former presence of menzerite-(Y) because of its similarity in composition and appearance to almandine that has cores of menzerite-(Y). There is no evidence for almandine being present when menzerite-(Y) was stable; it is only found as an overgrowth on menzerite-(Y). This absence is surprising given the relatively high bulk-rock Fe^{2+}/(Fe^{2+} + Mg) = 0.65 (E.S. Grew & J.H. Marsh, unpubl. data). Conditions for menzerite-(Y) crystallization are estimated to be $P \sim 7$–8.5 kbar and $T \sim 700$–800°C (Grew *et al.* 2010, Marsh *et al.* in prep.).

The absence of contacts of menzerite-(Y) with the major phases magnetite, oligoclase, quartz, augite and ferrosilite implies that menzerite-(Y) was no longer in equilibrium with these minerals at later stages of the metamorphism. We suggest that the breakdown of menzerite-(Y) is associated with partial melting, when it may have dissolved incongruently in the melt to give peritectic almandine. The incongruent dissolution resulted in cuspate outlines and even split single grains having an atoll-like appearance (Fig. 5a), whereas the sharp edges and smooth faces of the euhedral almandine (Fig. 4) are suggestive of crystallization from a melt. The melt subsequently crystallized K-feldspar in the moats. Alternatively, K-feldspar could have been a peritectic mineral that formed with almandine, or even have exsolved from ternary feldspar in the matrix. Conditions for dissolution of menzerite-(Y) are estimated to be $P \approxeq 8.5$–9.5 kbar and $T \approxeq 800$–850°C (Grew *et al.* 2010, Marsh *et al.* in prep.). Based on a comparison with diagrams in Petrík *et al.* (1995), Noyes *et al*. (1983) and Lindsley (1991), the $Fe^{3+}/\Sigma Fe = 0.36$ measured in allanite-(Ce) and up to 9 mol.% proportion of hematite solid-solution in ilmenite (E.S. Grew, J.H. Marsh & M.G. Yates, unpubl. data) suggest an oxygen fugacity roughly 1–2 $\log_{10}$ points more oxidizing than the quartz – fayalite – magnetite (QFM) buffer for the formation of menzerite-(Y).

CONCLUSIONS

The discovery of menzerite-(Y) and the garnet components $\{Y_2Ca\}[Mg_2](Si_3)O_{12}$ and $\{Y_2Ca\}[Fe^{2+}{}_2](Si_3)O_{12}$ in associated almandine adds a new dimension to the role of Y and HREE in garnet. Menzerite-(Y) may have been previously overlooked, because it resembles hercynite optically. The occurrence of menzerite-(Y) at Bonnet Island suggests that its formation and preservation require a distinctive set of circumstances, such as the absence of almandine during at least one stage of the metamorphic evolution, moderately oxidizing conditions and granulite-facies *P–T* conditions. We are less certain whether a high bulk Y + HREE content is critical. The host granulite contains 80.4 ppm Y, 12.7 ppm Dy, 9.85 ppm Er, and 11 ppm Yb (E.S. Grew & J.H. Marsh, unpubl. data on sample GB50), several times greater than most granulites.

Yttrium + REE substitution for divalent cations at the *X* site in menzerite-(Y) and associated almandine is balanced in charge largely by substitution of divalent cations for trivalent cations at the *Y* site, *i.e.*, ${}^{X}(Y,REE) + {}^{Y}R^{2+} = {}^{X}R^{2+} + {}^{Y}(Al,Fe^{3+})$, the menzerite substitution in Figure 9. Other substitutions that have been proposed for Y + REE incorporation in garnet, namely, ${}^{X}(Y,REE) + {}^{Z}(Al,Fe^{3+}) = {}^{X}R^{2+} + {}^{Z}Si$, the "yttrogarnet" substitution (*e.g*., Jaffe 1951), ${}^{X}(Y,REE) + {}^{X}Na = 2{}^{X}R^{2+}$ (Semenov 1963, Enami *et al*. 1995) or substitutions involving vacancies at the *X* site (Quartieri *et al*. 1999a, 1999b), play a subordinate or no role in the Bonnet Island garnets. The possibility that the menzerite substitution could also be important in the spessartine reported by Wang *et al*. (2003a, 2003b) suggests that this substitution could be widespread in metamorphic and igneous garnets overall.

ACKNOWLEDGEMENTS

We thank Frédéric Hatert, Vice-Chairman (changes in existing nomenclature) of the CNMNC IMA, for his comments on the nomenclature used in this paper. Comments by Charles Geiger, an anonymous referee and Robert F. Martin led to substantial improvement of the manuscript. JHM received support from a University of Maine Doctoral Research Fellowship. The research of ESG and MGY was supported by U.S. National Science Foundation grants OPP–0228842, EAR 0837980 and MRI–0116235 to the University of Maine, and that of MDD, by NSF grant EAR–0809459 to Mount Holyoke College.

REFERENCES

ABS-WURMBACH, I. & PETERS, T. (1999): The Mn–Al–Si–O system: an experimental study of phase relations applied to parageneses in manganese-rich ores and rocks. *Eur. J. Mineral*. **11**, 45-68.

ARMBRUSTER, T. (1995): Structure refinement of hydrous andradite, $Ca_3Fe_{1.54}Mn_{0.20}Al_{0.26}(SiO_4)_{1.65}(O_4H_4)_{1.35}$, from the Wessels mine, Kalahari manganese field, South Africa. *Eur. J. Mineral*. **7**, 1221-1225.

ARMBRUSTER, T., BIRRER, J., LIBOWITZKY, E. & BERAN, A. (1998): Crystal chemistry of Ti-bearing andradites. *Eur. J. Mineral*. **10**, 907-921.

ARMBRUSTER, T. & GEIGER, C.A. (1993): Andradite crystal chemistry, dynamic X-site disorder and structural strain in silicate garnets. *Eur. J. Mineral*. **5**, 59-71.

ARMBRUSTER, T., GEIGER, C.A. & LAGER, G.A. (1992): Single-crystal X-ray structure study of synthetic pyrope almandine garnets at 100 and 293 K. *Am. Mineral*. **77**, 512-521.

BACK, M.E. & MANDARINO, J.A. (2008): *Fleischer's Glossary of Mineral Species 2008*. The Mineralogical Record Inc., Tucson, Arizona.

BEA, F. (1996): Residence of REE, Y, Th and U in granites and crustal protoliths; implications for the chemistry of crustal melts. *J. Petrol*. **37**, 521-552.

BERRY, A.J., O'NEILL, H.ST. C., JAYASURIYA, K.D., CAMPBELL, S.J. & FORAN, G.J. (2003): XANES calibrations for the oxidation state of iron in a silicate glass. *Am. Mineral*. **88**, 967-977.

CULSHAW, N.G., JAMIESON, R.A., KETCHUM, J.W.F., WODICKA, N., CORRIGAN, D. & REYNOLDS, P.H. (1997): Transect across the northwestern Grenville orogen, Georgian Bay, Ontario: polystage convergence and extension in the lower crust. *Tectonics* **16**, 966-982.

DAVIDSON, A., CULSHAW, N.G. & NADEAU, L. (1982): A tectono-metamorphic framework for part of the Grenville Province, Parry Sound region, Ontario. *Geol. Surv. Can., Pap*. **82-1A**, 175-190.

DROOP, G.T.R. (1987): A general equation for estimating Fe^{3+} concentrations in ferromagnesian silicates and oxides from microprobe analyses, using stoichiometric criteria. *Mineral. Mag*. **51**, 431-435.

DYAR, M.D., LOWE, E.W. GUIDOTTI, C.V. & DELANEY, J.S. (2002): Fe^{3+} and Fe^{2+} partitioning among silicates in metapelites: a synchrotron micro-XANES study. *Am. Mineral*. **87**, 514-522.

ENAMI, M., CONG, B., YOSHIDA, T. & KAWABE, I. (1995): A mechanism for Na incorporation in garnet: an example from garnet in orthogneiss from the Su–Lu terrane, eastern China. *Am. Mineral.* **80**, 475-482.

GEIGER, C.A. (2004): An introduction to spectroscopic methods in the mineral sciences and geochemistry. *In* Spectroscopic Methods in Mineralogy (A. Beran & E. Libowitzky, eds.). *Eur. Mineral. Union, Notes in Mineralogy* **6**, 1-42.

GEIGER, C.A. & ARMBRUSTER, T. (1997): $Mn_3Al_2Si_3O_{12}$ spessartine and $Ca_3Al_2Si_3O_{12}$ grossular garnet: structural dynamic and thermodynamic properties. *Am. Mineral.* **82**, 740-747.

GEIGER, C.A., RUBIE, D.C., ROSS, C.R., II & SEIFERT, F. (1991a): Synthesis and ^{57}Fe Mössbauer study of (Mg,Fe) SiO_3 garnet. *Terra Abstr.* **3**, 63.

GEIGER, C.A., RUBIE, D.C., ROSS, C.R., II & SEIFERT, F. (1991b): A cation partitioning study of (Mg,Fe)SiO_3 garnet using ^{57}Fe Mössbauer spectroscopy. *Trans. Am. Geophys. Union* (*Eos*) **72**, 564-565 (abstr.).

GEIGER, C.A., STAHL, A. & ROSSMAN, G.R. (2000): Single-crystal IR- and UV/VIS-spectroscopic measurements on transition-metal-bearing pyrope: the incorporation of hydroxide in garnet. *Eur. J. Mineral.* **12**, 259-271.

GELLER, S. (1967): Crystal chemistry of the garnets. *Z. Kristallogr.* **125**, 1-47.

GIARAMITA, M.J. & DAY, H.W. (1990) Error propagation in calculations of structural formulas. *Am. Mineral.* **75**, 170-182.

GREW, E.S., MARSH, J.H. & YATES, M.G. (2010): A new yttrium-rich garnet species, $\{(Y,REE)(Ca,Fe^{2+})_2\}[(Mg,Fe^{2+})(Fe^{3+},Al)](Si_3)O_{12}$: implications for the prograde metamorphic path in the Parry Sound domain, Central Gneiss Belt, Grenville Orogenic Province. *Geol. Assoc. Can. – Mineral. Assoc. Can., Program Abstr.* <http://www.geocanada2010.ca/uploads/abstracts_new/160_GC2010_Abstract_final.doc>.

HARLEY, S.L. & KELLY, N.M. (2007): The impact of zircon–garnet REE distribution data on the interpretation of zircon U–Pb ages in complex high-grade terrains: an example from the Rauer Islands, East Antarctica. *Chem. Geol.* **241**, 62-87.

HATERT, F. & BURKE, E.A.J. (2008): The IMA–CNMNC dominant-constituent rule revisited and extended. *Can. Mineral.* **46**, 717-728.

HAWTHORNE, F.C. (2002): The use of end-member charge-arrangements in defining new mineral species and heterovalent substitutions in complex minerals. *Can. Mineral.* **40**, 699-710.

HÖFER, H.E., BREY, G.P., YAXLEY, G.M. & BERRY, A.J. (2006): Iron oxidation state determination in garnets by EPMA and XANES. *Geochim. Cosmochim. Acta* **70** (18 Supplement), A256 (abstr.).

ITO, J. (1967): A new yttrium magnesium silicate garnet, $Y_6Mg_5Si_5O_{24}$, and its rare earth and nickel analogues. *Mater. Res. Bull.* **2**, 1093-1098.

JAFFE, H.W. (1951): The role of yttrium and other minor elements in the garnet group. *Am. Mineral.* **36**, 133-155.

KASOWSKI, M.A. & HOGARTH, D.D. (1968): Yttrian andradite from the Gatineau Park, Quebec. *Can. Mineral.* **9**, 552-558.

KÜHBERGER, A., FEHR, T., HUCKENHOLZ, H.G. & AMTHAUER, G. (1989): Crystal chemistry of a natural schorlomite and Ti-andradites synthesized at different oxygen fugacities. *Phys. Chem. Minerals* **16**, 734-740.

LANZIROTTI, A. (1995): Yttrium zoning in metamorphic garnets. *Geochim. Cosmoschim. Acta* **59**, 4105-4110.

LAVES, F. (1962): The growing field of mineral structures. *In* Fifty Years of X-Ray Diffraction. Dedicated to the International Union of Crystallography on the occasion of the commemoration meeting in Munich, July 1962 (P.P. Ewald, ed.). A. Oosthoek's Uitgeversmij, Utrecht, The Netherlands (174-189).

LINDSLEY, D.H. (1991): Experimental studies of oxide minerals. *In* Oxide Minerals: Petrologic and Magnetic Significance (D.H. Lindsley, ed.). *Rev. Mineral.* **25**, 69-106.

LOCOCK, A.J. (2008): An Excel spreadsheet to recast analyses of garnet into end-member components, and a synopsis of the crystal chemistry of natural silicate garnets. *Comput. Geosci.* **34**, 1769-1780.

MANDARINO, J.A. (1981): The Gladstone–Dale relationship. IV. The compatibility concept and its application. *Can. Mineral.* **19**, 441-450.

MAO, H.K., BELL, P.M. & BOCTOR, N.Z. (1982): The mineral chemistry of majorite in L6 chondrites. *Carnegie Inst. Wash., Year Book* **81**, 279-281.

MEDENBACH, O. (1986): Ein modifiziertes Kristallbohrgerät nach Verschure (1978) zur Isolierung kleiner Einkristalle aus Dünnschliffen. *Fortschr. Mineral.* **64**, 113 (abstr.).

MENZER, G. (1925): Die Kristallstruktur von Granat. *Centralbl. Mineral. Geol. Paläontol. Abt. A, Mineral. Petrogr.* **1925**, 344-345.

MENZER, G. (1926): Die Kristallstruktur von Granat. *Z. Kristallogr.* **63**, 157-158.

MENZER, G. (1928): Die Kristallstruktur der Granate. *Z. Kristallogr.* **69**, 300-396.

MERLET, C. (1994): An accurate computer correction program for quantitative electron probe microanalysis. *Mikrochim. Acta* **114/115**, 363-376.

MOTTANA, A. (2004): X-ray absorption spectroscopy in mineralogy: theory and experiment in the XANES region. *In* Spectroscopic Methods in Mineralogy (A. Beran & E.

Libowitzky, eds.). *Eur. Mineral. Union, Notes in Mineralogy* **6**, 465-552.

NOVAK, G.A. & GIBBS, G.V. (1971): The crystal chemistry of the silicate garnets. *Am. Mineral.* **56**, 791-825.

NOYES, H.J., WONES, D.R. & FREY, F.A. (1983): A tale of two plutons: petrographic and mineralogic constraints on the petrogenesis of the Red Lake and Eagle Peak plutons, central Sierra Nevada, California. *J. Geol.* **91**, 353-379.

PETRÍK, I., BROSKA, I., LIPKA, J. & SIMAN, P. (1995): Granitoid allanite-(Ce): substitution relations, redox conditions and REE distributions (on an example of I-type granitoids, western Carpathians, Slovakia). *Geologica Carpathica* **46**, 79-94.

PYLE, J.M. & SPEAR, F.S. (1999): Yttrium zoning in garnet: coupling of major and accessory phases during metamorphic reactions. *Geol. Mater. Res.* **1**(6), 1-49.

QUARTIERI, S., ANTONIOLI, G., GEIGER, C.A., ARTIOLI, G. & LOTTICI, P.P. (1999a): XAFS characterization of the structural site of Yb in synthetic pyrope and grossular garnets. *Phys. Chem. Minerals* **26**, 251-256.

QUARTIERI, S., CHABOY, J., ANTONIOLI, G. & GEIGER, C.A. (1999b): XAFS characterization of the structural site of Yb in synthetic pyrope and grossular garnets. II. XANES full multiple scattering calculations at the Yb L_I - and L_{III}-edges. *Phys. Chem. Minerals* **27**, 88-94.

REINEN, D. (1964): Die Lichtabsorption des Co^{2+} und Ni^{2+} in oxidischen Festkörpern mit Granatstruktur. 1. *Z. Anorg. Allg. Chem.* **327**, 238-252.

RICKWOOD, P.C. (1968): On recasting analyses of garnet into end-member molecules. *Contrib. Mineral. Petrol.* **18**, 175-198.

RØHR, T.S., AUSTRHEIM, H. & ERAMBERT, M. (2007): Stress-induced redistribution of yttrium and heavy rare-earth elements (HREE) in garnet during high-grade polymetamorphism. *Am. Mineral.* **92**, 1276-1287.

RUBATTO, D. & HERMANN, J. (2007): Experimental zircon/melt and zircon/garnet trace element partitioning and implications for the geochronology of crustal rocks. *Chem. Geol.* **241**, 38-61.

SEMENOV, E.I. (1963): *Mineralogy of the Rare Earths*. Izdatel'stvo Akademii Nauk SSSR, Moscow, Russia (in Russian).

SETLUR, A.A., HEWARD, W.J., GAO, Y., SRIVASTAVA, A.M., CHANDRAN, R.G. & SHANKAR, M.V. (2006): Crystal chemistry and luminescence of Ce^{3+}-doped $Lu_2CaMg_2(Si,Ge)_3O_{12}$ and its use in LED based lighting. *Chem. Mater.* **18**, 3314-3322.

SMITH, J.V. & MASON, B. (1970): Pyroxene–garnet transformation in Coorara meteorite. *Science* **168**, 832-833.

SUWA, Y., NAKA, S. & NODA, T. (1970): Site preference of Mg^{2+} ion in $\{Y_{3-x}Mg_x\}[Mg_yAl_{2-y}](Al_{3-(x+y)}Si_{x+y})O_{12}$ garnet system. *Kogyo Kagaku Zasshi* **73**, 1936-1940 (in Japanese).

SUWA, Y., NAKA, S. & NODA, T. (1971): Determination of coordination states of Al^{3+} and Mg^{2+} in $\{Y_{3-x}Mg_x\}[Mg_yAl_{2-y}](Al_{3-(x+y)}Si_{x+y})O_{12}$ garnets by means of X-ray fluorescence spectral shifts. *Kogyo Kagaku Zasshi* **74**, 845-848 (in Japanese).

WANG, RU CHENG, FONTAN, F., CHEN XIAO MING, HU HUAN, LIU, CHANG SHI, XU, SHI JIN & DE PARSEVAL, P. (2003a): Accessory minerals in the Xihuashan Y-enriched granitic complex, southern China: a record of magmatic and hydrothermal stages of evolution. *Can. Mineral.* **41**, 727-748.

WANG, RUCHENG, HU, HUAN, ZHANG, AICHENG, XU, SHIJIN & WANG, DELI (2003b): Yttrium zoning in garnet from the Xihuashan granitic complex and its petrologic implications. *Chin. Sci. Bull.* **48**, 1611-1615.

WILDNER, M., ANDRUT, M. & RUDOWICZ, C.Z. (2004): Optical absorption spectroscopy in geosciences. I. Basic concepts of crystal field theory. *In* Spectroscopic Methods in Mineralogy (A. Beran & E. Libowitzky, eds.). *Eur. Mineral. Union, Notes in Mineralogy* **6**, 93-144.

WILKE, M., FARGES, F., PETIT, P.-E., BROWN, G.E., JR. & MARTIN, F. (2001): Oxidation state and coordination of Fe in minerals: an Fe *K*-XANES spectroscopic study. *Am. Mineral.* **86**, 714-730.

YODER, H.S. & KEITH, M.L. (1951): Complete substitution of aluminum for silicon: the system $3MnO•Al_2O_3•3SiO_2$ – $3Y_2O_3•5Al_2O_3$. *Am. Mineral.* **36**, 519-533.

YVON, K., JEITSCHKO, W., PARTHÉ, E. (1977) LAZY PULVERIX, a computer program, for calculating X-ray and neutron diffraction powder patterns. *J. Appl. Crystallogr.* **10**, 73-74.

Received December 15, 2009, revised manuscript accepted September 10, 2010.